A two-layer capacitor-based power management system for a stack of microbial fuel cells

by

Amirreza AZIMI

THESIS PRESENTED TO ÉCOLE DE TECHNOLOGIE SUPÉRIEURE
IN PARTIAL FULFILLMENT FOR A MASTER'S DEGREE
WITH THESIS IN ELECTRICAL ENGINEERING
M.A.SC.

MONTREAL, NOVEMBER 18, 2022

ÉCOLE DE TECHNOLOGIE SUPÉRIEURE
UNIVERSITÉ DU QUÉBEC

BOARD OF EXAMINERS

THIS THESIS HAS BEEN EVALUATED

BY THE FOLLOWING BOARD OF EXAMINERS

Ms. Lyne Woodward, Thesis Supervisor
Department of Electrical Engineering, École de technologie supérieure

Mr. Ambrish Chandra, President of the Board of Examiners
Department of Electrical Engineering, École de technologie supérieure

Mr. Vahé Nerguizian, Member of the jury
Department of Electrical Engineering, École de technologie supérieure

THIS THESIS WAS PRENSENTED AND DEFENDED

IN THE PRESENCE OF A BOARD OF EXAMINERS AND PUBLIC

ON OCTOBER 26, 2022

AT ÉCOLE DE TECHNOLOGIE SUPÉRIEURE

ACKNOWLEDGMENT

I would like to thank my supervisor, Lyne Woodward, ing, Ph.D., for her infinite support and guidance during this journey. It has been a great learning opportunity for me thanks to the experiences and the knowledge that she has shared with me. I will be employing the lessons I have learned under your supervision throughout professional career, and you have my eternal gratitude for it.

Although I didn't have the pleasure to work with Cong-Long Nguyen for an extended period, I would like to show my appreciation for his efforts in building and maintaining microbial fuel cells. This was the reason I was able to conduct measurements and have a hands-on learning experience with the devices that I was working on.

I would like to thank Mr. Vahé Nerguizian and Mr. Ambrish Chandra for taking the time to assess this thesis.

I would like to thank my dearest Ali Vedaei Sabegh, Soheil Pouraltafi Kheljan, and Alireza Kazemimanesh for not leaving my side, for the support, for the counsel, and for the constant encouragements.

Last but not the least, I would like to thank my family for all the sacrifices they have made so that I can follow my passion. It is all thanks to your loving, caring, and patient attitude toward me that I have been able to accomplish this work. Thank you for being there for me.

Un système de gestion de l'énergie basé sur deux couches de condensateurs pour un empilement de piles à combustible microbiennes

Amirreza AZIMI

RÉSUMÉ

Alors que le taux de pénétration des énergies renouvelables et durables augmente chaque jour, la demande de nouvelles sources et d'une récolte d'énergie plus efficace ne cesse de croître. Les piles à combustible microbiennes (MFC), en tant que source d'énergie durable, ont récemment attiré l'attention des scientifiques dans différents domaines. Cette source d'énergie alternative peut utiliser toute matière organique, y compris les eaux usées urbaines ou industrielles, comme combustible pour produire de l'énergie sans émettre de gaz à effet de serre comme sous-produit.

Compte tenu de la faible densité de puissance des MFC, il est très important de concevoir des systèmes de gestion de la puissance (PMS) efficaces et adaptatifs. Ces systèmes produiront une puissance et une tension utilisables pour la charge tout en gérant les fluctuations élevées des MFC. Cette étude vise à concevoir un nouveau PMS qui augmentera la puissance moyenne de sortie d'une pile du MFC en détectant celles qui sont défectueuses et à faible rendement ainsi qu'en les déconnectant de la pile. Dans cette approche, la puissance de sortie moyenne de diverses combinaisons d'états de commutation prospectifs et actuels est estimée et l'état de commutation qui donne une puissance de sortie plus élevée est sélectionné par le PMS. Bien que le retrait des MFC de l'empilement entraîne de faibles pertes potentielles sur une courte période après la déconnexion, il est important d'évaluer le fonctionnement du PMS à long terme. Afin de contrôler la fréquence, la précision et la robustesse du PMS ainsi que d'éviter les pertes potentielles, une méthode de contrôle par hystérésis, une approche de moyenne mobile simple et une période de repos ont été mises en œuvre. Ces méthodes de contrôle supplémentaires aident le PMS à ajuster sa tolérance aux MFC à faible rendement, à baser sa décision sur plusieurs cycles pour éliminer l'effet du bruit de mesure et à éviter les connexions et déconnexions répétitives.

L'énergie récoltée est envoyée à un convertisseur élévateur pour fournir une tension utilisable à la charge. Ce convertisseur survolteur aidera le PMS à augmenter l'amplitude de la tension de sortie et à réguler cette dernière à l'aide d'un contrôleur proportionnel intégral (PI).

Pour évaluer la performance de ce PMS, plus de 100 mesures ont été prises sur quatre MFC dans le laboratoire et deux cas de test ont été construits pour reproduire leur comportement par un simple modèle électrique équivalent basé sur ces mesures. Ces mesures ont été prises dans différentes conditions ambiantes et opérationnelles, de sorte que les cas de test peuvent représenter une grande variété de comportements des MFC. Ces cadres de test ont été générés dans MATLAB Simulink ® et le PMS proposé a été testé dans ce cadre de test. Bien que le PMS puisse gérer un nombre infini de MFC dans une pile, pour des raisons pratiques, une pile de quatre MFC a été choisie comme exemple. Les résultats montrent que le PMS proposé est capable de détecter et de déconnecter avec succès les MFC défectueux et peu performants de la pile, il est également résistant au perturbation électrique et qu'il parvient à augmenter le puissance de sortie moyenne par rapport à un PMS similaire proposé dans une étude antérieure (Nguyen, Tartakovsky, & Woodward, 2019). Le PMS proposé présente une augmentation de

puissance de sortie moyenne jusqu'à 67% sans régulation de tension et une augmentation jusqu'à 23% avec régulation de tension par rapport à l'étude précédente (Nguyen et al., 2019).

Mots clés : Pile à combustible microbienne (PCM), maximum power point tracking (MPPT), système de gestion de l'énergie, convertisseur élévateur, régulation de la tension.

A two-layer capacitor-based power management system for a stack of microbial fuel cells

Amirreza AZIMI

ABSTRACT

While the penetration rate of renewable and sustainable energies is growing daily, the demand for newer sources and more efficient energy harvesting has been growing. Microbial fuel cells (MFC), as a sustainable energy source, have gained a lot of attention recently from scientists in different fields. This alternative source of energy can use any organic matter including urban or industrial wastewater as fuel to produce energy and does not emit any greenhouse gas as a byproduct.

Given the low power density of MFCs, it is very important to design efficient and adaptive power management systems (PMS). These systems will produce usable power and voltage for load while managing high fluctuations of the MFCs. This study aims to design a new PMS that will increase the mean output power of the stack of MFCs by detecting faulty and low-performing MFC(s) and disconnecting them from the stack. In this approach mean power output of various prospective actions is estimated and the action that results in higher output power is selected by the PMS. Although removing MFC units from the stack causes small potential losses over a brief period after disconnection, it is important to evaluate the PMS in long-term operation. To control the frequency, accuracy, and robustness of the PMS and avoid potential losses, a hysteresis control method, a simple moving average approach and a cooldown timer have been implemented. These additional control methods help the PMS to adjust its tolerance to low-performing MFCs, base its decision on multiple cycles to eliminate the effect of noise in measurement and avoid repetitive connections and disconnections.

The harvested energy is then sent to a boost converter to deliver a usable voltage to the load. This boost converter will help the PMS to increase the magnitude of the output voltage and regulate the voltage using a proportional integral (PI) controller.

To evaluate the performance of this PMS, more than 100 measurements were taken from four MFCs in the lab and two test cases were constructed to replicate their behavior by a simple electrical equivalent model based on the measurements. These measurements were taken in different ambient and operational conditions, so the test cases can represent a wide variety of MFC behavior. This testing framework was implemented in MATLAB Simulink® and the proposed PMS was tested under this testing framework. Although the proposed PMS can theoretically manage an infinite number of MFCs in a stack, for practical reasons a stack of four MFCs was chosen as an example. The results show that the proposed PMS is able to successfully detect and disconnect faulty and low-performing MFC from the stack, is resistant to electrical noise and disturbances and manages to increase the mean output power compared to a similar PMS proposed by a former study (Nguyen et al., 2019). The proposed PMS presents an increase in mean output power of up to 67% without voltage regulation and an increase of up to 23% with voltage regulation compared to the former study (Nguyen et al., 2019).

Keywords: Microbial fuel cell, maximum power point tracking (MPPT), power management system, boost converter, voltage regulation.

TABLE OF CONTENT

Page

LIST OF TABLES

Page

LIST OF FIGURES

Page

LIST OF ABBREVIATIONS AND ACRONYMS

ADC	Analog To Digital
ANFIS	Adaptive Neuro Fuzzy Inference System
ANN	Artificial Neural Network
CEM	Cation Exchange Membrane
COD	Chemical Oxygen Demand
COD	Chemical Oxygen Demand
DC	Direct Current
EEC	Electrical Equivalent Circuit
IPCC	Intergovernmental Panel on Climate Change
MFC	Microbial Fuel Cell
MMSE	Minimum Mean Square Error
MPP	Maximum Power Point
MPPT	Maximum Power Point Tracking
ODE	Ordinary Differential Equation
P&O	Perturb and Observe
PDE	Partial Differential Equation
PEM	Proton Exchange Membrane
PI	Proportional Integral Derivative
PMS	Power Management System
PV	Photovoltaic

PWM	Pulse Width Modulation
SAMFC	Solid Anolyte Microbial Fuel Cell
SMA	Simple Moving Average
TEA	Terminal Electron Acceptor
UNFCC	United Nations Framework Convention on Climate Change

LIST OF SYMBOLS

V_{MFC}	Output voltage of the MFC
V_{OC}	Open circuit voltage of the MFC
C_i	Capacitor of the mfc_i
Vc_{Li}	Lower threshold for the C_i voltage
Vc_{Hi}	Higher threshold for the C_i voltage
SWA_i	Switch between mfc_i and C_i
SWB_i	Bypass switch of the C_i
SWBC	Boost converter switch
SC	Supercapacitor of the circuit
SWSC	Supercapacitor switch
R_1, R_2, C_{int}	Parameters of MFC electrical equivalent circuit
α	Interval between voltage measurements of online V_{OC} estimation
Δ	Offset between $V_{OC}/2$ and V_H or V_L as a percentage of V_{OC}
Δt_{ci}	Charge time of mfc_i
Δt_d	Discharge time stack
Δt_{total}	Total duration of a full charge-discharge cycle
E_i	Energy that C_i can deliver to the supercapacitor during the discharge period
E_{total}	Total energy that is delivered to the supercapacitor during the discharge period
$\overline{P_a}$	Mean power output of the system at the load level at the current state of the system
$\overline{P_b}$	Mean power output of the system at the load level if one MFC is discarded from the system

h	Hysteresis coefficient
m	Number of samples that SMA method uses to take average
RT	Reconnection cool off period for the discarded MFCs
D	Duty cycle of the boost converter
V_{in}	Input voltage of the boost converter
V_{out}	Output voltage of the boost converter
C_O	Output capacitor of the boost converter
R_L	Resistive load connected to the output of the boost converter
L	Boost converter inductor
F_{sw}	Switching frequency of the boost converter
K_p	Proportional element of the PID controller
K_i	Integral element of the PID controller

INTRODUCTION

It has been known to the science community for a while that the energy sources that once ignited the industrial revolution are not sustainable anymore. Recently, international organizations (like UNFCC and IPCC) have been trying to raise awareness about climate change and its short-term and long-term effects on our quality of life by holding conferences (Conference of Paris 2015) and publishing reports (special report on global warming of 1.5°C, 2018). Hence, renewable and sustainable energy sources have been gaining a bigger share in our day to day lives. However, this fast growth of renewable energy technologies is made possible by the efforts of the scientists who are finding new energy sources and ameliorating the efficiency and affordability of already existing technologies.

Microbial fuel cells (MFC) are a member of sustainable energy sources family just like photovoltaic (PV) cells and wind turbines, even though its power density is far less than the other sources. An MFC is a bioreactor where the bacteria grow and anaerobically digest the organic material present in the reactor. During this process and as a byproduct of a series of redox reactions, protons and electrons are released. These electrons can be extracted out of the cell and act as a source of electrical power while traveling through an external load. The advantage of this form of energy is that the "fuel" of this process, known as the substrate of the reactor can be any organic matter (including urban or some industrial waste) and the byproducts of the energy transform are ideally not harmful to the environment (usually only water). Since MFCs can digest organic matter, it has been shown that in small scales, MFCs can treat wastewaters with high organic material density like urban (Ge & He, 2016) and some food related industries (Feng, Wang, Logan, & Lee, 2008). These factors make MFCs clean and sustainable sources of energy that can be used not only for energy production but for wastewater treatment as well.

Although MFC technology is a clean source of energy, it has its own set of challenges that stand in the way of scaling and commercialization of this technology. Even though in the past two decades the power density of MFCs has been increased by a few orders of magnitude, it is still considered very low compared to other sources. Low power density prevents small MFC

stacks to supply power to typical electronic devices in a continuous mode. Moreover, attempts to increase the power output by increasing MFC volume did not succeed in producing the same power density in large volume reactors as in laboratory-scale reactors.

Many studies have been addressing the drawbacks of the MFC technology from different perspectives. One cluster of studies have been concentrated on improving the chemical and structural aspect of the reactor like shape, material, layout, etc., to increase the power density of the reactor (J. R. Kim et al., 2010). Some other studies have been focused on the biological aspect like the microorganism selection and inoculum, substrate material and concentration, etc. to improve the wastewater treatment efficacy and power output (Adekunle, Raghavan, & Tartakovsky, 2017). The third cluster of studies done in this domain are focused on what happens between the MFC and the load (J Coronado, Perrier, & Tartakovsky, 2013; Nguyen et al., 2019). These studies are mostly conducted by electrical and control engineers and attempt to maximize the energy output of the system without changing the nature of load or the source (MFC reactor). These studies attempt to optimize and improve the efficacy of the power production by designing power management systems (PMS) and output voltage boosters able to consider the behavior and limitations of the MFC and the intended load.

This study falls under the third cluster of studies. The author presents a new PMS that controls when and how the MFCs energy is harvested and how the voltage is boosted to supply the power needed by the electrical load connected at the output. Furthermore, this study proposes a new method to test the PMS and the voltage boosting method. In this testing method, several weeks of experimental data from MFCs is collected and then processed to provide an estimate of MFC behavior under different ambient and operating conditions, which can be used in simulation. By using this testing method, the control and voltage boosting system can be evaluated under a variety of real-world conditions in a cost-effective approach.

The contributions of this study are as follows:

- Development of a new PMS well adapted to a stack of MFCs;

- Design of a Boosting and regulating voltage system which takes into consideration the specific source and the load;
- Generation of multiple test cases based on a set of experimental data extracted from 4 laboratory scale MFCs operated under various operating conditions to validate the proposed PMS.

This thesis is organized in four chapters. In chapter one, a LITERATURE REVIEW, covers basic concepts of the MFC technology, the mathematical modeling of MFCs, the use of control and optimization in PMS, and voltage boosting methods used in prior studies in these fields. Chapter two, PROPOSED METHODOLOGY, comprises of several subchapters each explaining the details of the proposed PMS and voltage boosting and regulating method. Chapter three, EXPERIMENTAL DATA ACQUISITION AND PARAMETER ESTIMATION, demonstrate the steps taken in the experiments, the data processing procedure, and the construction of the MFC test cases to be used for validation purpose. Chapter four, SIMULATION AND RESULTS, illustrates the results of the tests carried out on the proposed PMS using the test cases constructed in chapter three and discusses the obtained results.

CHAPTER 1

LITERATURE REVIEW

It has been known to the science community for over a century that micro-organisms can produce electricity (Potter, 1911). Nevertheless, this subject didn't get much attention until the early 2000s. During the past two decades, more research has been done on different aspects of microbial fuel cells (MFCs) including its chemical, biological, material science, electrical, and control aspects. However, there is still a long way ahead before this technology becomes a commercially viable energy source for certain applications. Currently, the major impediments in the way of commercializing MFCs is their high construction cost, low energy density, and unpredictable nature of microorganisms.

1.1 Microbial fuel cells

1.1.1 Operation

Microbial fuel cell (MFC) is a biochemical reactor in which the microorganisms digest organic material and act as catalyst in an oxydo-reduction reaction where a small potential difference is produced between electrodes and a current flow through an electrical load connected between the 2 electrodes, producing electrical power in the process. Figure 1.1 shows a schematic of a two chambers MFC reactor. The process of voltage generation starts when the anodic chamber is inoculated by adding substrate material which contains bacteria, where colonies of bacteria inhabit the anode surface. The anode material must have certain properties in order to fulfill its function in the MFC: it should be highly conductive, non-corrosive, and should have high surface area per unit of volume (Logan, 2008). This will ensure that this environment is big enough and not toxic for the growth of the bacteria while being able to transfer the electrical charge out of the MFC.

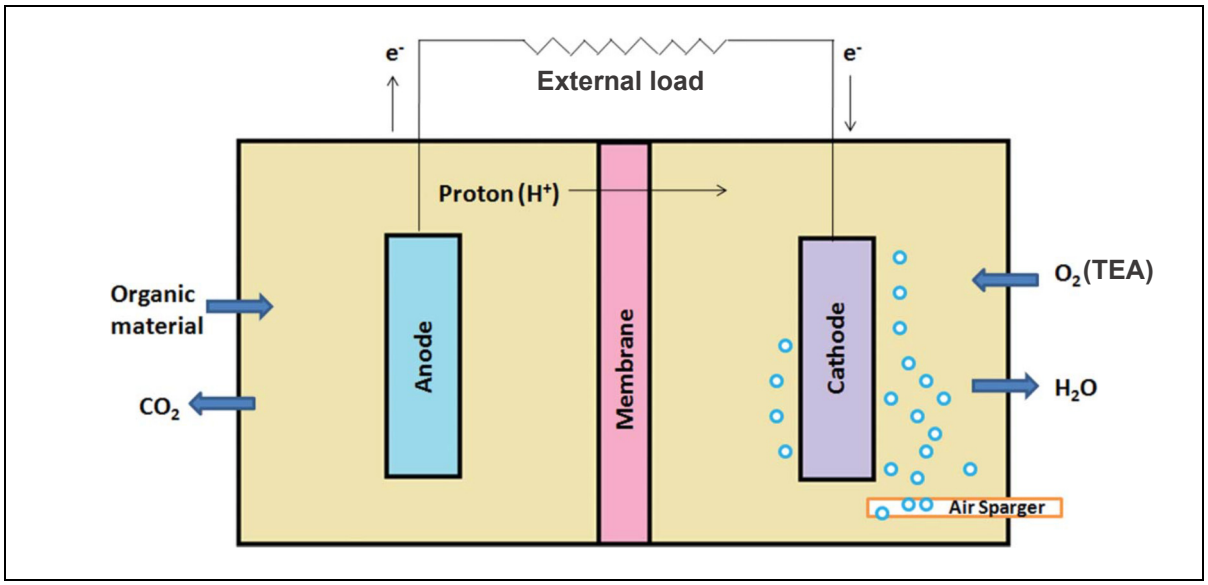

Figure 1.1 Schematics of a two chamber MFC reactor
Taken from Goswami and Mishra (2018)

Once the biofilm has covered the surface of the anode, within a few days of inoculation, the power extraction process can begin. The bacteria will start oxidizing the organic material inside the reactor while producing protons and free electrons in the process (equation (1.1)). The organic material can range from acetic acid to human or animal waste and can be introduced to the cell in batch, fed batch, or continuous process modes based on the type and application of the MFC reactor. Once the proton is produced in the anode, it travels in the reactor through the proton exchange membrane (PEM) up to the cathodic chamber while the electron travels through the outside wires (external load) to the cathode inserted into the cathodic chamber. In the cathodic chamber, the terminal electron acceptor (TEA), which is oxygen in the case of Figure 1.1, gets reduced (equation (1.2)) and diffuses out of the cell (Logan, 2008). Although there are various options for TEA like nitrate and sulfate, the most accessible one is oxygen that can be reduced to water. In the case of two chamber MFCs, the oxygen can be introduced by actively pumping it inside the cathodic chamber. The travel of the electrons from the anode to the cathode terminal generates a current that can run through potential electronic devices and power them. Respectively, cathode and anode reactions assuming the substrate material is acetic acid, can be formulated as described in equations 1.1 and 1.2 (Goswami & Mishra, 2018):

$$\text{Anode: } CH_3COO + 2H_2O \xrightarrow{Microorganisms} 2CO_2 + 7H^+ + 8e \quad (1.1)$$

$$\text{Cathode: } O_2 + 4e + 4H^+ \xrightarrow{\text{Catalyst}} 2H_2O \quad (1.2)$$

The bacteria that are able to digest organic matter and transfer the produced electrons directly outside the cell without the need for a solution, mediator or an immediate TEA are called "exoelectrogens". This type of bacteria is what make the MFC function as it should, the higher the number of such bacterial colonies as a percentage of the total bacterial population on the biofilm the higher the efficiency of the MFC (Logan, 2008).

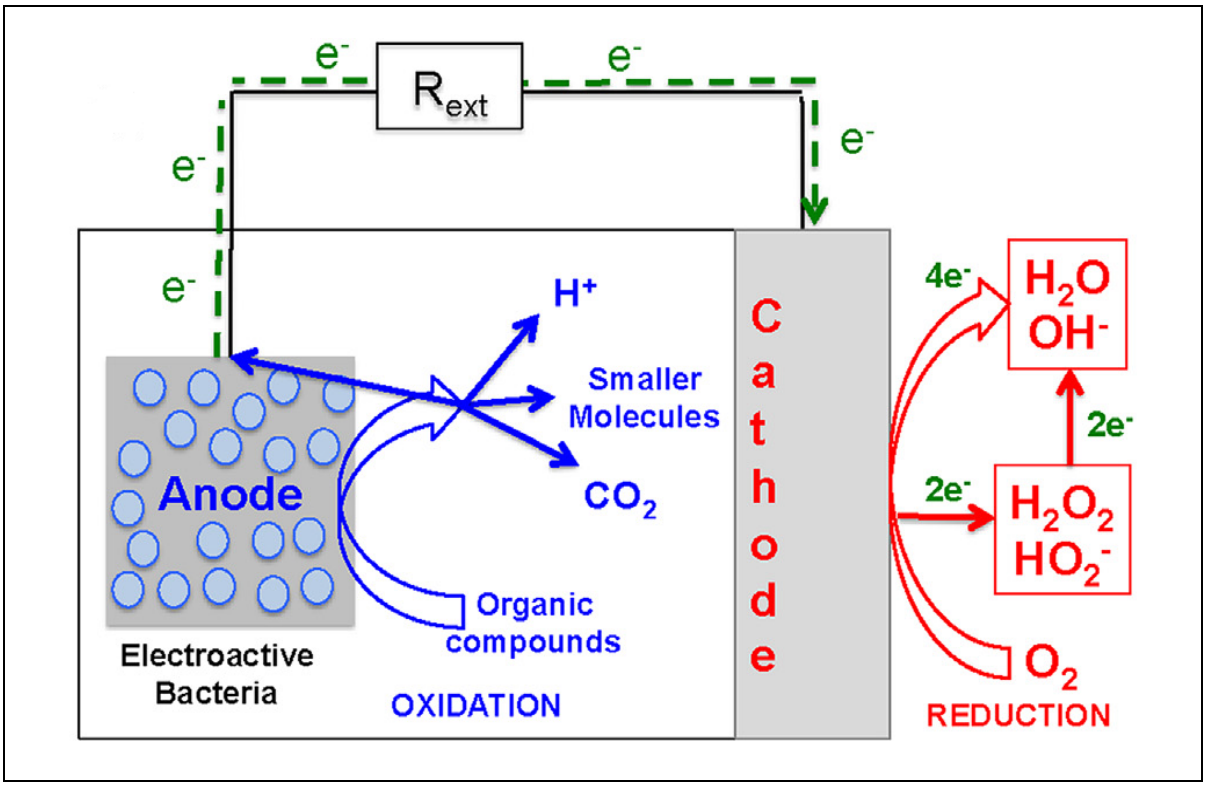

Figure 1.2 Schematics and chemical reactions occuring in a single chamber MFC
Taken from Santoro, Arbizzani, Erable, and Ieropoulos (2017)

Another simpler form factor of the MFC reactors, namely single compartment air-cathode reactors, are illustrated in Figure 1.2. The reason the two chambers were separated by a PEM in the previously mentioned two-chamber reactors was the fact that the digestion of organic

matter in the anodic chamber is an anaerobic process, hence the oxygen in the cathodic chamber needs to be kept away from the place the degradation of organic matter happens. The single compartment form factor has been reported to be more practical, cheaper and easier to scale-up due to the elimination of the PEM and incorporation of the catalysts in the electrodes while producing approximately similar power output compared to two-chamber MFCs (Park & Zeikus, 2003). Although the single compartment structure has its own advantages, there are certain disadvantages like higher rate of aerobic digestion due to the presence of oxygen and harder leakage management (Logan, 2008). More recent studies have used wet proof carbon paper air cathodes to let the oxygen in while keeping the water inside the reactor (Cheng, Liu, & Logan, 2006).

The substrate material can also be a determining factor in the properties of MFCs. While it is necessary for the anaerobic digestion of organic matter by the bacteria to happen while submerged in water, the source of the organic material can be solid itself. Studies have shown that using solid anolytes that release organic matter into the anode compartment, have lower degradation rates and can last potentially for years if need be (Adekunle et al., 2017). Solid anolyte MFCs (SAMFC) are most useful in cases where constant maintenance and feeding of the MFCs is not possible or justifiable, since they can function only on one batch of substrate for long periods. However, since all the organic matter is not readily available at all times, these types of MFCs have lower power densities than their “liquid-based” counterparts.

1.1.2 Application

For a very long time MFCs were considered as a purely scientific topic with no real applications. However, in the past decade, the potential of MFC in multiple applications have been shown the literature. These application range include (but not limited to): electricity generation, wastewater treatment (removing organic and inorganic material), chemical extraction, and biosensing.

1.1.2.1 Electricity generation

Electricity generation has been the most interesting aspect of MFCs for researchers since the early 2000s (J. Wang, Zheng, Wang, Xu, & Wang, 2015) and it will be the main interest of this study as well. Since the early days of MFC development, scientists have been trying to prove the practical value of MFCs in providing energy for real applications. Some of these attempts have been presented in (I. Ieropoulos, Melhuish, Greenman, & Horsfield, 2005; Min, Kim, Oh, Regan, & Logan, 2005; Shantaram, Beyenal, Veluchamy, & Lewandowski, 2005).

One of the main use cases of MFCs have been supplying energy for low power telemetry systems and environmental sensors like temperature, humidity (D. Zhang, Yang, Shimotori, Wang, & Huang, 2012), salinity, etc. in remote areas (Shantaram et al., 2005). These areas are generally hard to reach and supplying power without constant need to change/charge batteries is a big challenge. MFCs seem to be good solution for this challenge since, they work for extended periods until they run out of substrate material to feed on. This prolonged functioning, eliminates the need to change or charge batteries. Researchers has shown how different substrates can have different effects on the longevity and power production of the MFCs and how mixing different organic material can boost power while increasing the longevity at the same time. Adekunle et al. (2017) compared four carbon sources for power production and longevity and concluded that between sawdust, peat moss, humus, and cattle manure the best performing SAMFC would be the one made from sawdust and humus mixture. In this combination, humus is considered as a source of microorganisms and primary source of carbon and saw dust is considered as a slow releasing source of carbon for longevity. In this study, they were able to harvest energy for over 9 months from the MFC with sawdust and humus substrate material.

For sea floor applications, sediment MFCs can be good choices, since the organic material is being replaced in the sediments by the water current, these MFCs have been shown to function for long periods without human intervention (Mitov, Bardarov, Mandjukov, & Hubenova, 2015) and can theoretically function forever.

MFC systems like the one used in EcoBot-III has also been able to eliminate any need for human intervention (I. Ieropoulos, Greenman, Melhuish, & Horsfield, 2010). However, it uses MFC generated power to feed itself, hence leaving less power available for other possible applications.

1.1.2.2 Water treatment

One of the most studied applications of MFCs is their wastewater treatment capabilities. In this application, the organic substrate material is made up of municipality sewage, sludge (Behera & Ghangrekar, 2009), humane urine (I. Ieropoulos, Greenman, & Melhuish, 2012), animal waste (Zhuang et al., 2012), wastewater from different industries or any kind of wastewater. In this application, the electricity generation is treated as a byproduct of the main goal which is water treatment, mineral extraction (Kuntke et al., 2012), and pathogen killing (I. Ieropoulos, Pasternak, & Greenman, 2017). In such applications, the wastewater either flows through a cascade of multiple MFCs (Ge & He, 2016) or recirculates in the same MFC for multiple cycles (I. Ieropoulos et al., 2012) and at each step, a portion of the organic matter is digested by the bacteria producing CO_2, water, and electricity as a byproduct (in ideal conditions where the digestion is completely done anaerobically by exoelectrogen bacteria). Wastewater treatment studies have shown 60%-90% COD removal from wastewater while producing small amount of electricity. Although most of these studies are done using miniature sized prototype (mostly smaller than 1L), there have been attempts at higher volume MFC units as well.

Ge and He (2016) reports a field trial of a 200-liter module made up of 96 individual MFCs using wastewater from a local water treatment facility. They reported to have reached 75% reduction in COD, 90% reduction in suspended solids during more than 300 days of operation with hydraulic retention time of 18h. Although the power is low, the total cost of this module was comparable to small-scale water treatment plants. Considering the fact that 60% of the material cost was spent on the cation exchange membrane (CEM) it is probable that in the future by using different CEM material or reduction of the price of CEMs the cost of small MFC treatment plants can be even lower.

A mix of both applications has been commercialized under the name of “PEE POWER®”. This technology started at University of the West of England when they started using urine as the substrate for their MFCs (I. Ieropoulos et al., 2012) and were able to harvest electrical energy, extract minerals, and treat the wastewater at the same time. This idea was scaled up (432 MFCs) and passed field trials (I. A. Ieropoulos et al., 2016) being able to provide the lighting, during the night time, for the urinals only using the extracted power from the urine fed MFCs. This technology has since been implemented in two rural schools one in Nairobi, Kenya and one in rural Uganda. The reports have confirmed that the MFC module in rural Ugandan school has been in operation for 8 months through multiple types of impact like rust, long periods of inactivity, clogging, or excess humidity (FuelCellsWorks, 2018; UWE-Bristol, 2018).

1.2 Mathematical modeling of microbial fuel cells

Deb, Patel, and Balas (2020) categorizes the MFC modeling approaches in two major categories: fundamental approach and application-based approach. In order to represent the dynamic behavior of the MFC in the fundamental approach, differential equations are used. Some of these models simplify the model to lumped-parameters and use ordinary differential equations (ODE) (Recio-Garrido, Perrier, & Tartakovsky, 2016), whereas more accurate models use distributed parameters and partial differential equations (PDE) (Picioreanu, Katuri, van Loosdrecht, Head, & Scott, 2010) to represent time and spatial dimensions of the MFC reactor . The fundamental approach is the most accurate approach to modelling MFCs and can formulate many variables and reactions happening in the reactor like substrate consumption, redox reactions in anode and cathode compartments, emf dynamics, biofilm formation, electrical values etc.

1.2.1 MFC modeling by fundamental approach

(X.-C. Zhang & Halme, 1995) published one of the first fundamental models of the MFC using a double chambered MFC. They acknowledged the fact that MFCs are very complex systems

partly due to the abundance of reactions occurring at the same time each with a different time constant and dynamic. Therefore, they make some assumptions to simplify the problem based on their previous observations (Halme & Zhang, 1995). They assume that the mediator is not dissociated by bacteria, electrolyte concentration is high and it's homogeneous in the solution, mass transfer is fast enough not to cause any limitation, abundance of the material in cathode compartment and cathodic reactions are fast enough not to be a bottleneck. Given such assumptions, the growth of the bacteria and consumption of substrate are described by ODE based on Monod equation. The redox reactions inside the bacteria and at the surface of the electrode are also considered first order reactions. This model recognizes two distinct time constants for the MFC, one to replicate fast electrical responses and one longer time constant to represent slower chemical reactions. This study calculates the potential difference between the two electrodes based on electrochemistry rules (Nernst equation). Moreover, three voltage drop sources were recognized in this model, ohmic, concentration, and activation. However, the effect of concentration voltage drop is deemed to be ignorable.

More recent models using fundamental approach have attempted to increase the accuracy of the MFC model by considering two (Recio-Garrido et al., 2016) or multiple (Picioreanu, Head, Katuri, van Loosdrecht, & Scott, 2007) bacterial communities, considering a membraneless single-chamber MFC instead of dual-chambered (Pinto, Srinivasan, Manuel, & Tartakovsky, 2010), considering the effect of cathode reactions (Esfandyari, Fanaei, Gheshlaghi, & Mahdavi, 2017), considering mediatorless MFCs (Oliveira, Simões, Melo, & Pinto, 2013), or considering spatial dimensions and mass transfer dynamics (Picioreanu et al., 2010)

1.2.2 MFC modeling based on application

Although models based on fundamental approach can be very accurate, they need multidisciplinary knowledge of MFCs for correct implementation and require high computational power. Application-based approach does not require an extensive knowledge of MFCs and does not require high computational power. These models concentrate more on the parameters that are being studied.

One of the most common application-based MFC models is the electrical equivalent circuit (EEC) model. This model is the most useful when the electrical behavior and interaction of the MFC with other electrical elements is being studied. In this study, this model is the best choice since the focus of this study is on the performance of MFC in a PMS circuit and its control. These models were inspired from lead acid battery models, some of which are presented in the study by Dürr, Cruden, Gair, and McDonald (2006) and different variations were first adopted in electrical behavior analysis study of MFCs (Liang, Huang, Fan, Cao, & Wang, 2007) and PMS study of MFCs (Yang, Zhang, Shimotori, Wang, & Huang, 2012).

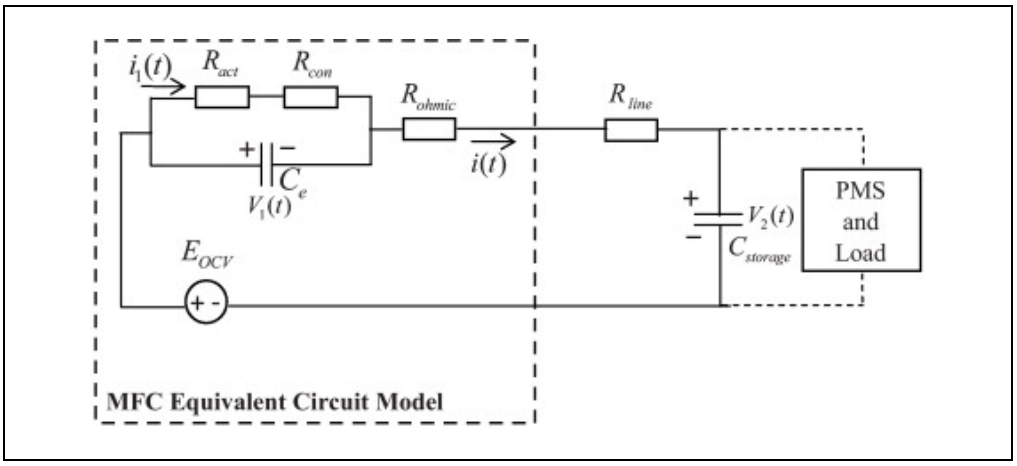

Figure 1.3 One of the first adopted EEC of MFCs
Taken from Yang et al. (2012)

The PMS study (Yang et al., 2012) points out how each resistor in the model presented in Figure 1.3 represents one source of loss in MFCs and how the capacitor represents the capacitance between the electrodes of the MFC. The electrical equivalent model introduced in Yang et al. (2012) have multiple resistors in series which can be simplified into one equivalent resistor for simplicity even though each single resistor represents a different source of energy loss. This simplified model depicted in Figure 1.4 was introduced by Javier Coronado, Tartakovsky, and Perrier (2013) and currently serves as the most popular model in PMS studies.

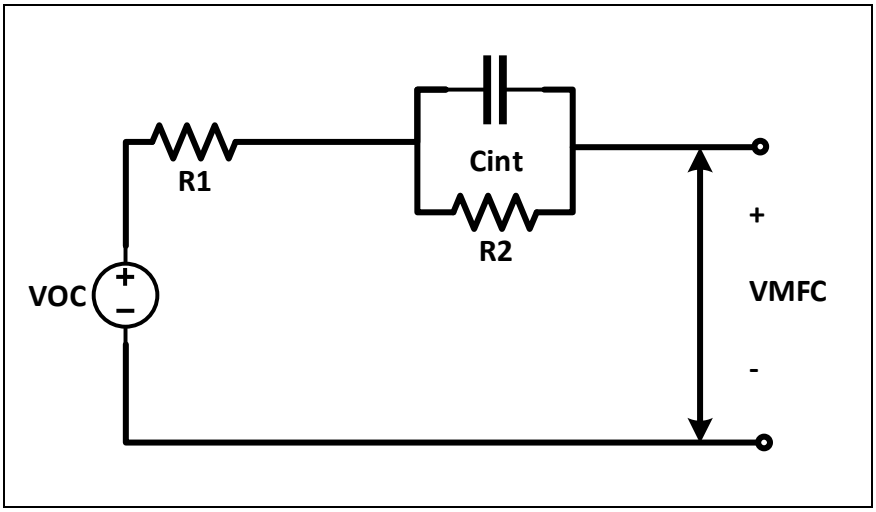

Figure 1.4 Simplified electrical equivalent circuit model of the MFC

Using electrical equivalent model of MFC provides details about MFC's behavior in the circuit without complicating the model with unnecessary details about chemical or biological aspect of the MFC and helps the simulations run faster (which is a huge obstacle in the case of this study). Although the chemical and biological aspects of the MFC affects the value of elements in the electrical equivalent model, once the values are estimated (by methods explained in section 3.1.4), the behavior of the MFC is represented only by the electrical equivalent elements.

Another example of application-based approach can be seen in (Esfandyari, Fanaei, Gheshlaghi, & Mahdavi, 2016), where machine learning technics like artificial neural network (ANN) and adaptive neuro fuzzy inference system (ANFIS) is used to model the MFC behavior and forecast its behavior in the future. These models need a substantial amount of historic data from each MFC to be able to accurately forecast the output. (Esfandyari et al., 2016) have been using four indicators as input: ionic strength, nitrogen concentration, pH, and temperature of the reactor and considers the power density to be the output of the model. Although this approach to modeling can be very accurate, however it takes a considerable amount of time to gather data for training the algorithm and is computationally expensive. These specifications make such models useful in MFC structure optimization studies rather than the studies that use MFCs only as power sources.

Model identification is very useful in both of these approaches and is applied when a model is already described in constants and variables. In this stage, a statistical approach is utilized to determine the values of the parameters in the model. This is done by taking numerous measurements from the MFC in different conditions and plugging in the measured input and output values in the model to solve it for the parameters. (X.-C. Zhang & Halme, 1995) used a mean square method in Simulink to determine the value of the missing parameters in their model. (Recio-Garrido et al., 2016) determined the constants by minimizing the difference between the experimental and simulated results using "fmincon" function in MATLAB.

1.3 Energy harvesting from microbial fuel cells

Power management systems or PMS are a series of circuit elements and control methods designed to optimize the functionality of energy sources and shape the harvested energy into practically usable energy. Optimization of energy sources is defined as maximizing the output power extracted for that source at any moment. However, in some applications like wastewater treatment, it can mean increasing the digestion rate by controlling the current (Rabaey et al., 2006).

Power management systems are necessary for using renewable energy systems in real-world setups in order to maintain a usable output power level. PMS systems are used in renewable energy systems to compensate for one of the biggest shortcomings of these systems, uncertainty, and fluctuation.

1.3.1 Application of PMS in Renewable energy systems

Unlike other energy sources (e.g., thermal power plants or hydro-electric generators), where you can control the output power, in the nominal range, by controlling the influx of fuel (or water in case of a hydro-electric dam), the influx and characteristics of the energy (solar irradiation, wind speed, or organic matter and bacterial activity) that renewable energy generators (like PV cell, wind turbine, and MFC) are exposed to are not controllable. Hence,

renewable energy sources cannot have a consistent or even accurately predictable output power. Solar irradiation can change instantaneously due to a shadow cast by a foreign object on the PV cell like an animal, a leaf, or a cloud. Although wind speed and direction can be forecasted days ahead, the forecasts are not always accurate. The same principle of uncertainty applies to MFCs as well, where although the material and concentration of the substrate can be controlled and manipulated, the behavior of the bacterial colony and consequently, the output power of an MFC can never be accurately foreseen.

One of the most important priorities of PMSs is to maximize the harvested power from the source based on the maximum power transfer theorem. This theorem states that to extract the maximum energy from an energy source, the external impedance needs to match the internal impedance of the source. Although the maximum power transfer theorem identifies the external impedance as the determining factor, the impedance that the energy source sees through its terminals can be manipulated by changing the load value, duty cycle of the boost converter, or controlling the voltage or the current at which, the energy source is harvested. For any energy source, at any given time, based on the ambient and internal conditions of the energy source, there is a specific operating point that yields maximum power transfer out of the energy source. This operating point is where the internal and external impedances match.

1.3.2 Single MFC power management technics

Typically, renewable energy sources have V-I and P-R curves similar to those shown in Figure 1.5 where the peak of the power curve is called the “maximum power point” (MPP). The algorithm that controls the operating point in real-time and forces it to track the MPP in real-time despite disturbances is called the maximum power point tracker (MPPT).

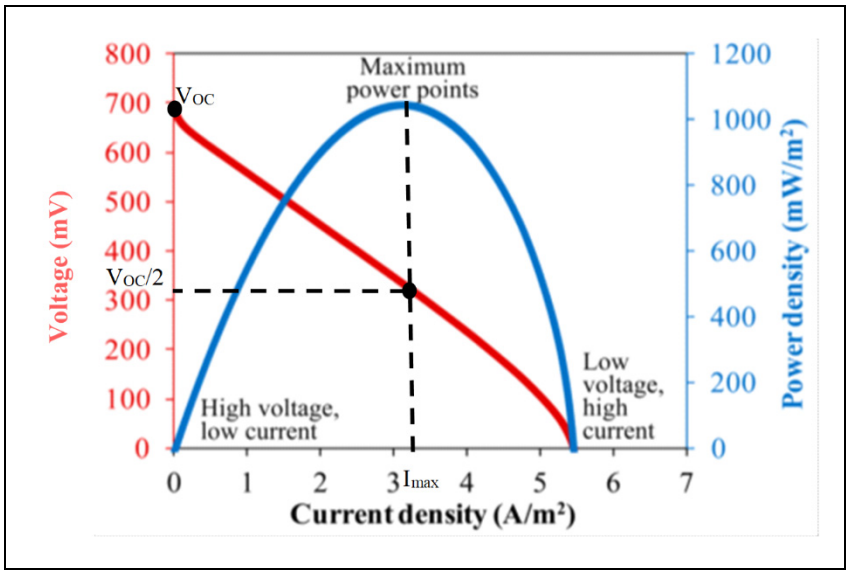

Figure 1.5 General form of static curvesfor MFCs
Taken from H. Wang, Park, and Ren (2015)

There are two parameters that characterizes the MPPT algorithms. First, the variable that is being manipulated to control the external impedance seen by the energy source, and second, the optimization algorithm that is being used to maintain the operating point at the MPP. Although it has been used in literature numerous times (J Coronado et al., 2013; Kebir, Woodward, & Akhrif, 2019), in real-world applications, using a variable resistor as a load is not a viable option. In most real-world applications there is a converter to boost the voltage of the energy source and/or regulate the output voltage of the system to serve the load needs. Having a boost converter in the circuit allows the PMS to use the duty cycle of the converter to control the impedance seen by the energy source. Using the duty cycle as the MPPT variable is the most popular in the literature.

The optimization algorithms used in maximum power point trackers can be categorized in five groups:

First group: Methods based on constant parameters: these methods use a predefined MPP and force the system to operate in that operating point regardless of the ambient conditions (Yu, Jung, Choi, & Kim, 2004). This is the most primitive group of tracking methods and has a very low implementation cost, however it is not very accurate. These methods manage to keep the

system in the vicinity of MPP, but it's practically impossible for them to track the true MPP. The parameters of this group need to be tuned based on the specific energy system they are going to control;

Second group: Methods based on measurement and comparison: these methods use a few predefined MPPs based on different ambient conditions and set the operating point based on the saved prior data (Y. Kim, Jo, & Kim, 1996). This is a more accurate tracking method than the previous group, however its accuracy is highly dependent on the number of prior samples stored in its memory. The methods in this group need digital sensors and computing power to read and compare data. They also need to be specifically tuned as well.

Third group: Methods based on trial and error: Mainly branched from perturb and observe (P&O) method (Pandey, Dasgupta, & Mukerjee, 2008), these are the most popular tracking methods used in the literature and industry, as well. The idea behind the operation of this group is that the algorithm makes a small perturbation in the system, observes the output results, and adjusts the next perturbations in accordance with the results of the previous step. For example, the tracking algorithm increases the duty cycle by a small mount, if the output power increases, the perturbation of the duty cycle was in a favorable direction, so the algorithm keeps increasing the duty cycle until the increase in duty cycle doesn't increase the power output anymore. On the other hand, if the increase in the duty cycle resulted in a decrease in the output power, then the perturbation was not in a favorable direction, so the algorithm keeps reducing the duty cycle until the reduction of duty cycle doesn't result in an increase in the power output. The size and frequency of the perturbation steps and adaptability of them are a big area of research and can be tuned to specific applications. Implementation of this group of tracking methods is generally easy and less costly since it doesn't need much computational power, is robust and can function even with minimal tuning. Multiunit optimization is another example of such algorithms (Woodward, Tartakovsky, Perrier, & Srinivasan, 2009). One of the disadvantages of this group of MPP trackers is the trade-off between convergence speed and convergence accuracy, that is, the larger the perturbation size is the shorter the convergence time but the lower the convergence precision. The other disadvantage is the constant chattering even after converging to the MPP. Although, these disadvantages can be alleviated by more

adaptive methods (Femia, Petrone, Spagnuolo, & Vitelli, 2005), the addition of such complexities would need more advanced computational resources.

Fourth group: Methods based on mathematical calculations: these methods are dependent on the mathematical model of the energy source or can identify the MPP by doing calculations based on the input and observed output. In the case of a solar cell connected to a boost converter, for instance, the tracker measures temperature, irradiance, and other variables (depending on the complexity of the mathematical model) and determine the MPP and the operating point that the PV needs to function at (Solodovnik, Liu, & Dougal, 2004). However, given the fact that there are numerous indeterminable factors in some energy sources like bio-electrochemical reactions in the MFCs, there is always going to be model mismatch between the mathematical model and the real-world system. Although these methods are fast to determine the MPP, their usage in much complicated energy systems like MFCs can be limited due to model mismatch. In such cases, model free algorithms that function only based on input and output analysis can excel in this particular field. Multiunit optimization is an example of such algorithms aimed at optimizing multiple units with similar dynamics (Woodward et al., 2009). This algorithm operates the units with a preset offset, determines the gradient between the output of the units caused by the offset, and forces the gradient to zero. It's important to note that the calculated gradient is not temporal (e.g. extremum-seeking method) but rather along the dimension of the unit. This feature enables multiunit algorithm to converge faster than temporal perturbation-based algorithms, since it doesn't need the units to reach steady state to update the input (as long as the dynamics of the units are identical). Although, the algorithm pushes the units towards MPPT, since the units are operated at an offset, one unit would converge to slightly above and the other below the MPP.

Fifth group: Methods based on intelligent prediction: the last group of MPPT algorithms are the intelligent methods. These methods are typically very fast in detection and convergence to the MPP and are very reliable. However, three examples of this group that are discussed here have serious drawbacks that need proper justification before use. The first method is a fuzzy logic tracking method which requires a high computational power to function and run the control algorithm in real-time (Kottas, Boutalis, & Karlis, 2006). The second method is a

neural network method which requires a historic data to train and tune the algorithm accurately for the specific system it's going to be connected to, which makes it hard to be implemented in a newly installed system (Hiyama, Kouzuma, & Imakubo, 1995). Even in previously installed systems, the characteristic of the energy source is going to change over time, so there is a need for periodic retuning of the tracking method. The third method is a particle swarm optimization algorithm which considers each PV module as a particle in the swarm which is being controlled individually to attain optimum of the bigger system (Chassé & Woodward, 2016). Since this algorithm is controlling each individual PV cell in the system, there is a lot of potential to increase the output power of the system compared to other methods of MPPT. Nevertheless, the number of switches and other components necessary to have control over every single module is going to affect the cost of implementation significantly.

Another output power optimization method that has been mentioned in the literature besides the MPPT methods, is intermittent connection of the energy source to the load (PWM operation). This method is specifically used in MFC energy systems and is reported to increase the output power by 22-43% (J Coronado et al., 2013). In this method, instead of continuous connection of the MFC to the energy harvesting circuit, a switch is placed between the MFC and the circuit, and it's fed with a low frequency (>100Hz) PWM signal making the switch opens and closes repeatedly. This intermittent connection of the MFC to the circuit ameliorates the output power of the MFC and although the exact reason for this increase in performance is not clear, an analogy between catalytic reactors which were operated intermittently (Silveston, Hudgins, & Renken, 1995) and MFCs that are operated in the same way suggests that this mode of operation increases bio-catalytic activity. This heightened catalytic activity is believed to lead to reduction of two of the known sources of loss in MFCs, concentration and activation losses (J Coronado et al., 2013).

1.3.3 Multiple MFC configuration

Although online optimization techniques help to increase the efficiency of the MFC system, the power output or reliability of a single lab-scale MFC module in most cases is not enough to continuously power common electronic devices over a long period. Moreover, scaling up

MFC modules doesn't increase the power output linearly as expected, since the power density reduces as the volume increases due to the increase in the internal resistance as seen in the 16L MFC used by Jiang et al. (2011). (Logan, 2010) explains that the way to increase the power density is to increase the total electrode area per unit of volume in each MFC. Hence, the solution for the low voltage and power is to stack up multiple smaller MFC modules to power electronic devices at a constant voltage. The electrical connection between the MFC units in a stack can be separated into four categories: parallel, series, series/parallel, isolated. Parallel connections can be beneficial for PMS systems only with a boost converter since the voltage of the stack is going to be relatively low for any practical load. Moreover, another bigger problem in such connections is the possibility of voltage reversal caused by different terminal voltage of MFCs. This phenomenon is very likely to happen in this configuration and is very dangerous for the general well-being of the MFCs. Series connections would output higher voltages and prevent voltage reversal problem between MFCs. In systems where voltage stability is not as important, these systems can connect directly to the load without having to boost the voltage with a converter. However, in case one of the MFCs stops working (due to contamination, depletion of substrate, physical damage, etc.) the whole system would stop delivering energy since the flow of electricity is broken in the series connection. Parallel/series connections are seen mostly in bigger energy systems where, the system comprises of many MFC modules. These energy systems are made up of clusters of MFCs in parallel, where inside each cluster, MFCs are connected in series as seen in Figure 1.6.

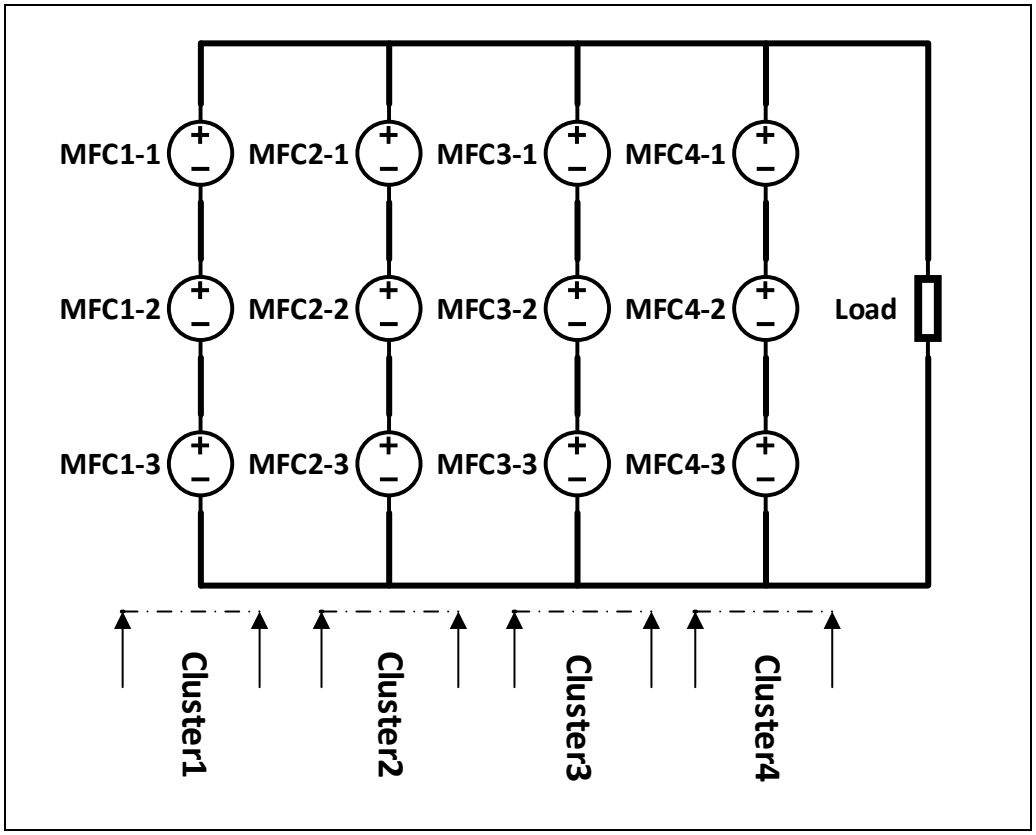

Figure 1.6 Configuration of a series/parallel MFC stack

This configuration increases the voltage of the stack to a usable level and prevents total blackout of the system by having several clusters as back up for a faulty cluster. As an instance, in the system in Figure 1.6, if one MFC in cluster 2 is faulty, cluster 2 would stop contributing to the power output of the system but the load will be powered with cluster 1, 3, and 4 still working. The isolated configuration of MFCs is possible when each MFC is directly connected to the PMS circuit. Typically, in this configuration, the MFCs charge separate capacitors, when the capacitors are charged, they get disconnected from the MFC and pass on the energy to the rest of the circuit. The capacitors connected to the MFCs can be connected in series or parallel themselves when they are being discharged to the rest of the circuit, this way, the system can benefit from the advantages of series or parallel connections without endangering the wellbeing of the MFCs. However, implementing this method requires much more components like switches to connect and disconnect and multiple capacitors or charge pumps.

1.3.4 Voltage boosting strategies

In the previous subsections we discussed how it is possible to boost voltage by configuring the MFCs themselves in a series connection. In this subsection, we are going to discuss the configuration of PMS elements that can help the energy harvesting system to boost voltage and overcome some of the main obstacles mentioned in the previous section, i.e., voltage reversal and system blackout in stacks with series connections where one system is malfunctioning. One of the most popular PMS configurations is the capacitor-based configuration (Ledezma, Stinchcombe, Greenman, & Ieropoulos, 2013). This configuration makes use of capacitors as a transitional energy storage between the energy source and the load, where the energy harvesting happens in multiple stages (MFCs to the capacitor(s), capacitor(s) to the load).

The simplest configuration connects a single capacitor to each MFC through a switch and provides intermittent connection and power delivery to the load. If there are several MFC units, their capacitors can be in series configuration while delivering power. This kind of connection although uses multiple switches and capacitors, provides multiple advantages like, higher power input from MFCs due to intermittent connection, preventing voltage reversal or any outside unwanted parameter to affect the MFC, and higher load voltage due to configuring the capacitors in series (Khaled, Ondel, & Allard, 2014). Other varieties of capacitor based PMSs can have multiple layers of capacitors to boost and stabilize the voltage before delivering it to the load (Nguyen et al., 2019).

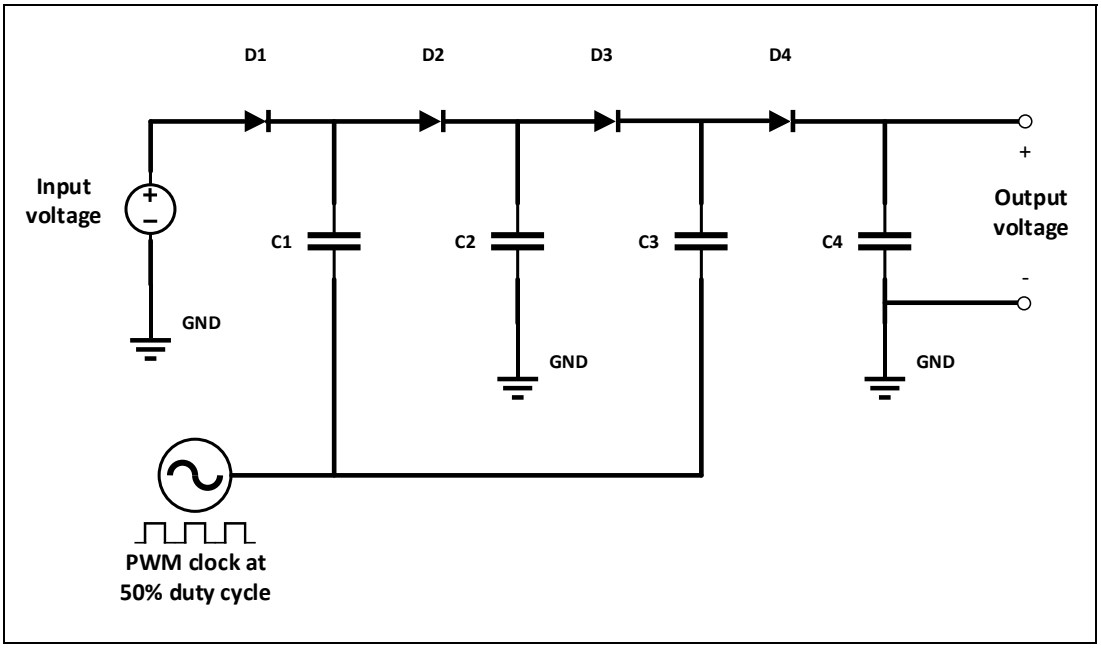

Figure 1.7 An example schematic of a 4 layer charge pump

Charge-pumps are used quite often in PMSs (Karra et al., 2014). As presented in Figure 1.7, charge pumps are DC-DC boost converters that use layers of capacitors to boost voltage instead of using an inductor. They use switching technics to reach different levels of voltage and can reach efficiency of 95%. In the scope of power management systems, they are primarily used for voltage boosting rather than stabilization or isolating MFC devices, unlike capacitors. Although high efficiency makes them favorable for low power applications, they have certain shortcomings that limit their usage in real-world applications. The first disadvantage of charge pumps is that their voltage boosting is only in discrete steps rather than on a continuous spectrum like boost converters. Most charge pumps control the output voltage by adding or removing capacitive layers, which will change the boost ratio only in integer values (e.g. 1:2, 1:3, 1:4). This makes regulating output voltage of charge pumps impossible without adding voltage regulation modules and eliminates them as a viable option for voltage sensitive loads. On the other hand, charge pumps can face problems when fed with very small voltage levels from a single MFC system. Since they are semiconductor-based electronics, very small amount of voltage from a single MFC may not even be able to reach the charge-pumps minimum input voltage level and therefore interrupt the flow of power.

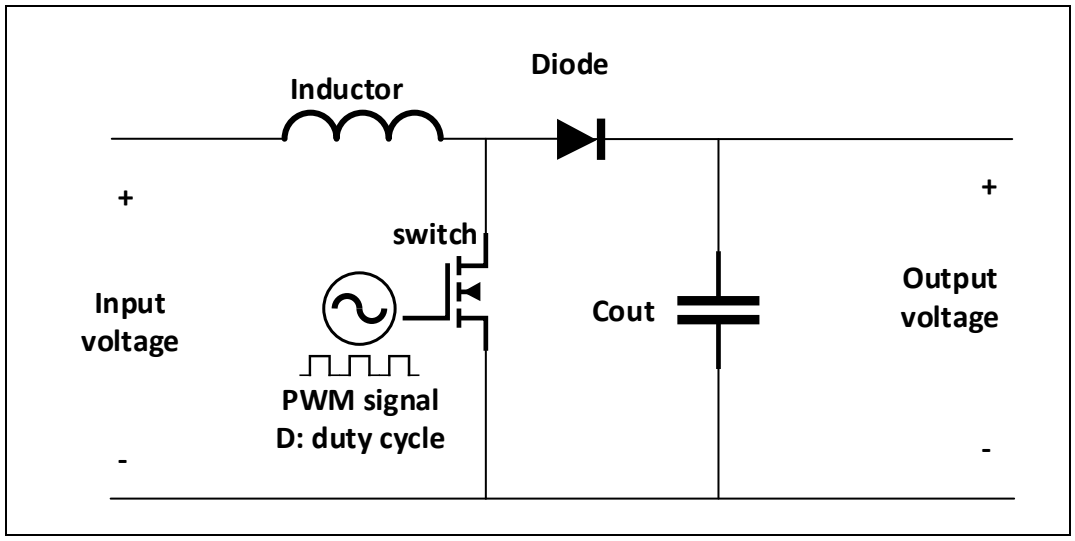

Figure 1.8 Schematic of a simple DC-DC boost converter

For the cases in which the voltage stability is necessary, the other voltage boosting option is the use of boost converters. Boost converters come in different forms and configurations but the main feature that makes them suitable for voltage boosting is their variable boost ratio. A simple example of boost converters is illustrated in Figure 1.8, in which the MFC voltage is fed to the input and the load is fed through the output terminal of the converter. The boost converter in Figure 1.8 have two phases, and these two phases are determined by the state of the switch which is receiving a PWM in its gate. Phase one is where the switch is closed, and the inductor is being charged by the input voltage source, acting as a load to the input voltage source. The second phase starts when the switch opens and due to the sudden change in the flow of current, a much bigger voltage compared to the input voltage level is induced on the terminals of the inductor in the opposite polarity. Consequently, the inductor starts acting as a source alongside the input voltage rather than a load in the circuit. In the second phase, the voltages of the input and the inductor add up together and produce a larger voltage and charge the output capacitor, which in turn supplies the load connected at the output terminal. Once the switch closes again (due to a high in the PWM signal at the gate of the switch), phase one restarts, the polarity of the inductor changes, and gets charged by the input voltage source once again. This process repeats and after a few cycles, the output capacitor voltage level reaches a steady state. This steady state voltage level is mandated by the duty cycle of the switch gate

PWM signal. According to equation (1.3), the higher the duty cycle, the higher the boost ratio will be.

$$\frac{V_{out}}{V_{in}} = \frac{1}{1 - D} \tag{1.3}$$

Although the values of inductor and switching frequency play a big role in converter design, efficiency, maximum power, etc., once the converter is built and set up, the only facture determining the boost ratio is the duty cycle. This feature coupled with output voltage level measurement and a control algorithm can be useful for voltage regulation. Several examples of such voltage regulation have been presented in the literature (X. Zhang et al., 2014), where the output voltage of the boost converter is kept fixed while the input voltage is fluctuating by manipulating the duty cycle of the PWM signal. Since the input voltage is boosted once in the inductor before reaching the semi-conductor (diode), boost converters can function with lower input voltages than charge-pumps.

The control of the boost converter plays a significant role in the efficacy of the voltage regulation; however, more accurate and more complex control algorithms also need more advanced processors and consequently consume more power as well. In an autonomous MFC system, where the PMS, load, and other electronics are/ powered by the MFC(s), the control algorithm needs to consume as little power as possible, due to the scarcity of the power in such systems. Therefore, it is important to recognize the trade-off and choose the algorithm according to the available processing and power limitations of an MFC powered system.

The most popular control method used in boost converters is the proportional integral derivative (PID) controller (Mumtaz et al., 2021). This controller is simple to implement in practice and can function in wide range of applications. This method requires minimum number of measurement signals to function, which is an important factor in the selection of the processor. Smaller processors with fewer ADC (analog to digital converter) ports, consume less power, which counts as an advantage for the PID control algorithm. The three coefficients of the PID method (k_p, k_i, k_d) needs to be specifically tuned for each system, however, using

the values tuned for a similar system (e.g., another MFC energy harvesting system in the same voltage level) can show acceptable results.

In conclusion, this chapter discusses many types of MFCs and materials used to build them in order to illustrate the fundamentals of MFC functioning (i.e. anode, cathode, frame, etc.). The next section of the chapter reviews the mathematical models that may be used to explain the characteristics of MFCs as well as the benefits and drawbacks of each model. The final section of this chapter discusses PMSs and voltage boosting techniques by providing a list of energy harvesting approaches used in earlier research and their limitations.

CHAPTER 2

PROPOSED METHODOLOGY

2.1 Introduction

Capacitor-based configurations have high practical potential since they provide higher voltage levels in short bursts, making them more useful for some applications. Remote sensing and measurement devices perform repetitive tasks in time intervals, making them a suitable use case for capacitor-based configurations. Since MFC (microbial fuel cell) units provide low power output to the PMS (power management system), it is essential to ensure that the used PMS harvests and delivers maximum energy to the load at any moment. Given the low power output, this study's objective has been to optimize the PMS design and operation in order to improve the energy harvesting system's efficiency.

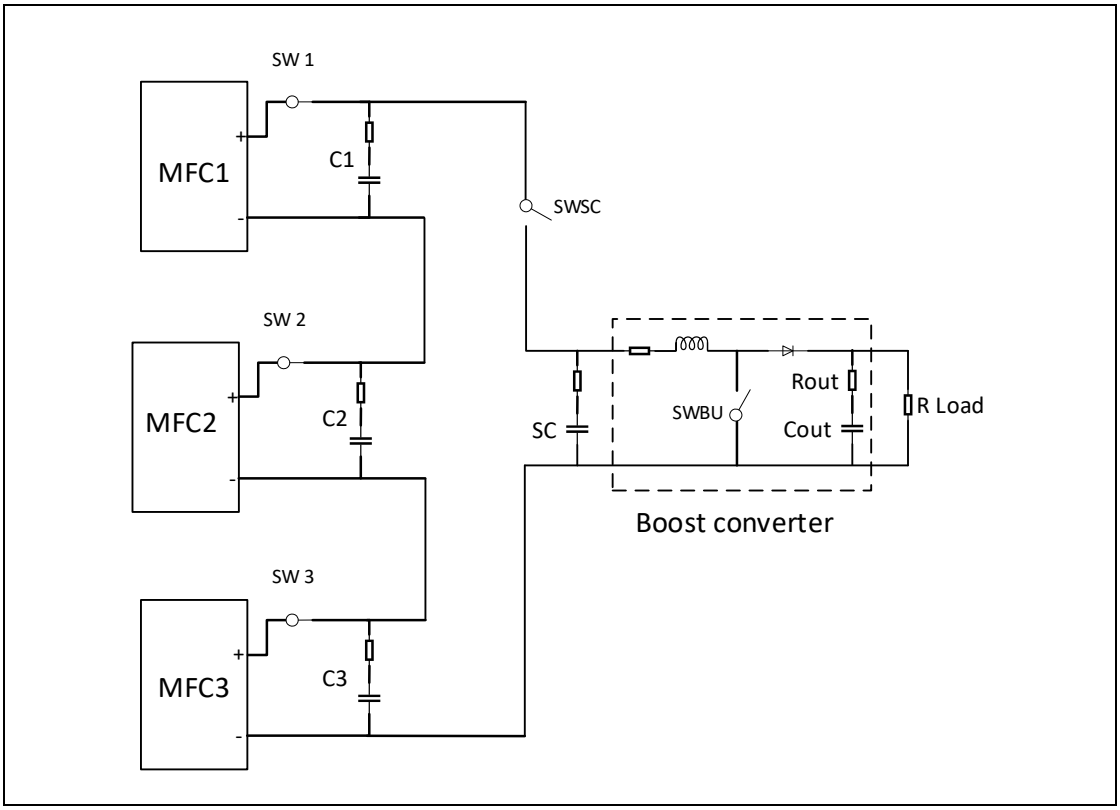

Figure 2.1 Topology of the PMS proposed in Nguyen et al. (2019)

The method presented in (Nguyen et al., 2019) is an excellent example of capacitor-based PMS presented in Figure 2.1. In this PMS, each MFC_i is connected to one capacitor C_i through a switch. The idea behind this PMS is to charge the C_i capacitors individually by their MFCs. Once all the capacitors are charged to a certain level, the switch between C_i and the MFC opens and the switch between the C_i capacitors and the supercapacitor closes. This lets the C_i capacitors to discharge to the super capacitor in series with a voltage higher than each individual capacitor. Once the C_i capacitors voltage levels drops to a certain level the SWSC opens and the SW_is close to restart the charging of C_is.

This is a very efficient PMS, however, operation under certain conditions leads to the loss of potential energy. Although this method can be used with non-identical MFC units, it would be the most efficient with identical units. Nevertheless, from a practical point of view, MFCs' behavior depends on living organisms that are constantly evolving. Consequently, it is almost impossible to replicate an MFC exactly. MFC units can experience significant differences in dynamics, voltage, and power output between one another regardless of how similar they were built, inoculated and maintained. Therefore, it is fair to assume that in a setup including multiple MFC units, as shown in Figure 2.1, MFCs would not charge simultaneously the capacitor they are attached to. Since this method requires all the units to start charging and discharging their capacitor simultaneously, the PMS will not take any action until all the capacitors are charged to a certain voltage threshold. An example of this occurrence during a simulation is pictured in Figure 2.2. During the period that units 2 and 3 are waiting for unit 1 to charge its capacitor, potential energy is not harvested. Let Δt_{ci} be defined as the time spent by unit *i* to charge C_i, and Δt as the total time spent in the charging phase, which is equal to Δt_{ci} of the slowest unit. It is observable that Δt-Δt_{c2} is when unit 2 is idle, and Δt-Δt_{c3} is the period where unit 3 is idle. For example, during these "idle" periods, MFCs 2 and 3 are isolated from the rest of the circuit, and no energy transfer or storage occurs. In the example shown in Figure 2-1, since MFC 1 is the slowest unit to charge its capacitor, it hinders the energy harvesting process of the MFC stack.

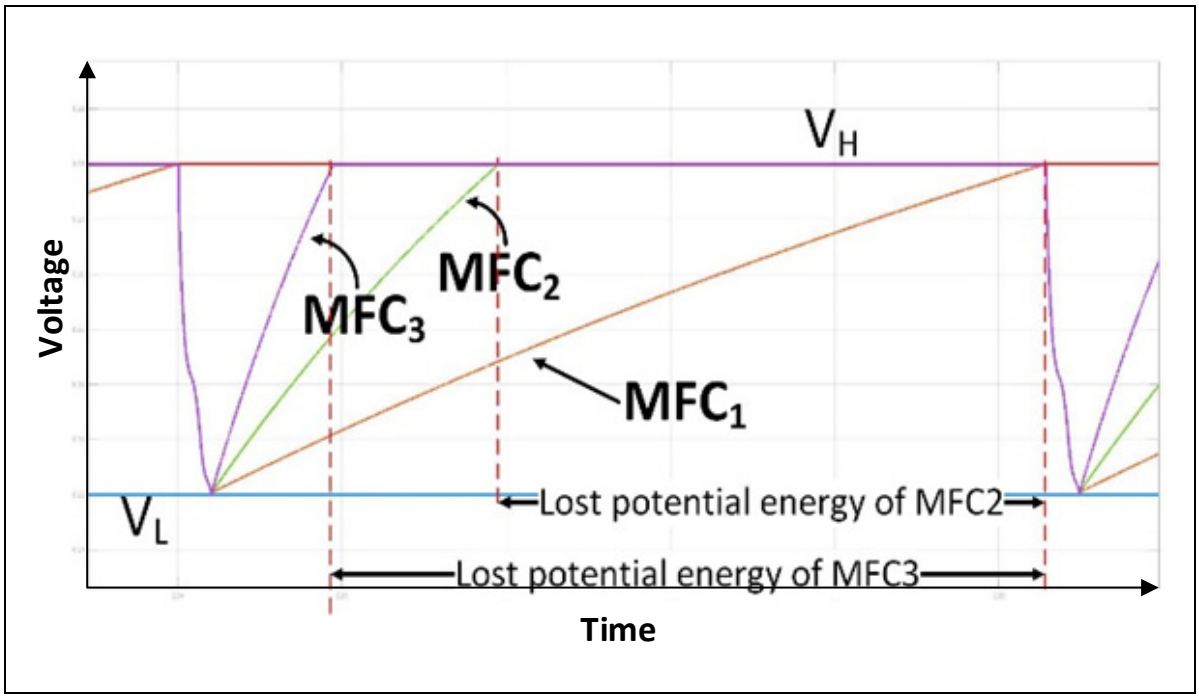

Figure 2.2 Example: MFC voltage levels during a charge-discharge cycle with non-identical MFCs

In some instances, the slowest unit can cause more energy loss than energy gain, since it's hindering the whole energy harvesting process by its long charge time. The proposed method presents a solution to this problem. If one MFC is slowing down the whole process and the resulting energy loss is more significant than the energy gain of that unit, the slowest unit can be discarded, which will result in a potential gain of total harvested energy over a long period.

A bigger problem presents itself in practical use once one of the MFC units stops charging its capacitor due to failure, rupture, or lack of organic material (substrate) inside the MFC or due to an electrical malfunction (disconnected wires, broken switches, etc.). In this condition, the algorithm would stop delivering power, possibly permanently, waiting for the malfunctioning unit to charge its capacitor.

The proposed circuit configuration is shown in Figure 2.3, where each unit has an extra switch to make the physical and electrical aspects of bypassing possible. When the algorithm decides to bypass unit *i,* SWB_i closes to short circuit unit *i*, and SWA_i opens and disconnects MFC to

avoid short-circuiting and harming MFC. In the example switch configuration presented in Figure 2.3, SWA_1 is opened and SWB_1 is closed to discard MFC_1 from the energy harvesting process while other MFC units have their SWA_i closed and SWB_i opened so they can charge their C_i capacitors. "Discarding algorithm" is responsible for the decision-making aspect of the proposed method.

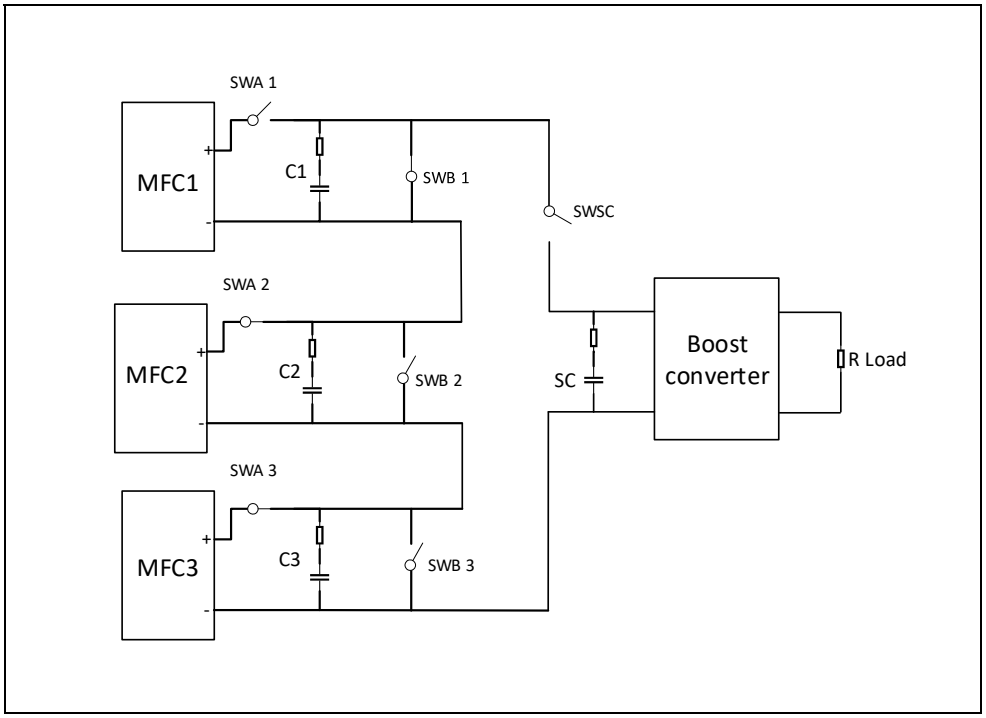

Figure 2.3 Circuit topology of the proposed method while MFC_1 is discarded from the circuit and the other units are charging their C_i capacitor

The objective of the proposed algorithm is to maximize the harvested energy over long-term operation. One way to approach this objective is to model the MFC with an equivalent electrical circuit (depicted in Figure 1.4) and estimate the values of the elements in the equivalent circuit. This way, the algorithm can use the maximum power transfer theorem and maximize the power received by C_i. However, to minimize the model mismatch in the process, the discarding algorithm utilizes an implicit real-time optimization approach solely based on the physically measurable parameters like MFC output voltage, delivered energy, and the charging duration of C_i capacitors.

To make a decision, the algorithm needs to perform the steps discussed in sections 2.2 to 2.4.

2.2 Maximum power point tracking

While an MFC unit is working and providing power, its internal characteristics change continuously due to the changes in its internal conditions. As an example, the microorganisms in the reactor are constantly oxidizing the organic matter and producing water as a byproduct, diluting the solution in the reactor. This affects the concentration of the organic matter and the speed of reactions, contributing to a change in the MFC internal resistance (Recio-Garrido et al., 2016). The procedure in which the output voltage of the power generating source is manipulated in order to harvest the maximum power in real-time is called maximum power point tracking (MPPT). Typically, MPPT is achieved by manipulating the load value, however, any form of voltage control can be used to push the power source to function at its maximum power point. Although an MPPT algorithm is not essential to the operation of a power production system, it significantly increases the system's efficiency.

Based on the maximum power transfer theorem, the external impedance needs to match the internal impedance to transfer the maximum power. Hence based on Figure 1.4, V_{OC} voltage would be evenly distributed between internal and external elements in such a way that $V_{MFC} \approx V_{OC}/2$. The practicality of this conclusion for MFC units is studied in the literature (H. Wang et al., 2015) and illustrated in Figure 1.5 by an example static curve.

V_{OC} is a potential difference on the equivalent circuit presented in Figure 1.4, however, it is not accessible for measurement in a real MFC unit. While the MFC is isolated from the rest of the circuit for a long time, it can be claimed that $V_{MFC} \approx V_{OC}$ since there is no electrical current running through the MFC and hence no voltage drop at internal elements. After connecting the unit to an external load, the output voltage of the MFC (V_{MFC}) would no longer be equal to V_{OC}. While being connected to a load, to control V_{MFC} as a function of V_{OC}, the value of V_{OC} needs to be estimated. In this study, the "online estimation of V_{OC}" presented by Nguyen et al. (2019) will be implemented. Considering the EEC model of the i^{th} MFC unit shown in Figure 1.4, V_{MFC} can be described as follows:

$$V_{MFC_i}(t) = V_{OC_i} - V_{C_{int}} e^{-t/\tau} \quad (2.1)$$

$V_{C_{int}}$ is the voltage across the internal capacitor (C_{int}), and τ is the time constant of the circuit. Since the MFC is disconnected from its capacitor, $\tau = C_{int} R_2$. Utilizing equation (2.1) and using three measurements of V_{MFC} taken in short intervals of time, we will have:

$$V_{MFCi}(t_0) = V_{OCi} - V_{Cint} e^{-t_0/\tau} \quad (2.2)$$

as first measurement, at time $t=t_0$,

$$V_{MFCi}(t_0 + \alpha) = V_{OCi} - V_{Cint} e^{-(t_0+\alpha)/\tau} \quad (2.3)$$

as second measurement, α seconds later at $t= t_0+ \alpha$, and

$$V_{MFCi}(t_0 + 2\alpha) = V_{OCi} - V_{Cint} e^{-(t_0+2\alpha)/\tau} \quad (2.4)$$

as third measurement, α seconds after the second measurement at $t= t_0+2\alpha$.
The first measurement takes place when SWA_i is opened, which is marked as t_0. If the constant α is much smaller than τ, it can be concluded that V_{OC} is constant between measurements, and therefore, the value of V_{OCi} can be calculated by solving the system of equations (2.2) to (2.4) for V_{OCi}:

$$V_{OCi} = \frac{V_{MFCi}(t_0)V_{MFCi}(t_0 + 2\alpha) + V_{MFCi}^2(t_0 + \alpha)}{V_{MFCi}(t_0) - 2V_{MFCi}(t_0 + \alpha) + V_{MFCi}(t_0 + 2\alpha)} \quad (2.5)$$

The main advantage of this method is that it relies solely on three V_{MFC} measurements and does not require any knowledge of V_{Cint}, C_{int}, or R_{int}.

2.3 SWA control method

Once the V_{OC} for each unit is determined, the upper and lower thresholds are set individually. As shown in equations (2.6) and(2.7), these thresholds are defined with a small constant offset ($\pm\Delta$) from $V_{OCi}/2$ to keep the voltage level close to half of the V_{OC} value and transfer the maximum power from MFC to its external capacitor C_i. Typically, the value of Δ is in order of 0.05, which means the upper and lower thresholds are 5% above and below $V_{OC}/2$ value, respectively.

$$V_{Hi} = V_{OCi}\left({}^{1}/_{2} + \Delta\right) \tag{2.6}$$

$$V_{Li} = V_{OCi}\left({}^{1}/_{2} - \Delta\right) \tag{2.7}$$

To fulfill the condition of MPP, the algorithm keeps the MFC output voltage and V_{Ci} between V_{Hi} and V_{Li} thresholds. According to Nguyen et al. (2019), the algorithm controls V_{MFC} using switches to charge and discharge capacitors according to these voltage thresholds. The algorithm closes the SWA_i if V_{MFCi} is below the lower voltage (V_{Li}) threshold so that C_i can charge (charging state of the system) and opens SWA_i if V_{MFCi} is above the upper voltage (V_{Hi}) threshold. Once all the SWAs are opened and all the C_i capacitors are charged to their V_{Hi}, SWSC closes. Closing SWSC configures C_i capacitors in series and discharges them into C_{sc}, lowering C_i voltage levels (discharging state of the system). A full cycle is defined from the beginning of the charging state to the end of discharging state of the system. During the discharging state, units start discharging their C_i capacitor simultaneously and reach their V_{Li} level simultaneously. This is very important since they are all connected in series, it is not possible to disconnect one before another. Therefore, to make sure the time it takes them to reach from V_{Hi} to V_{Li} is the same for every unit, the equation $C_1\Delta_1 V_{OC1} = C_2\Delta_2 V_{OC2} = \cdots = C_n\Delta_n V_{OCn}$ must be satisfied. Where *n* represents the total number of units. If capacitors have similar capacitance and V_{OC} is estimated for each unit, by setting Δ_1 to a fixed value (5% as recommended by the original study), the value Δ for other units can be calculated and updated

frequently. When units reach their lower threshold level, SWSC opens, all the SWAs close, and the charging state starts again increasing C_i voltage levels.

2.4 SWB control method

The main contribution of the proposed method would be to improve the PMS efficiency presented in Nguyen et al. (2019) in case MFC units are not identical. Due to the dynamic nature of MFCs, even similar units will perform quite differently, such differences can grow even larger over time as they continue to function. For instance, in the previous method, if in a stack of multiple MFCs, one MFC unit is much slower than others to charge its C_i capacitor, faster MFCs would wait idle until this slowest MFC finishes charging its capacitor.

In cases where the differences between MFC units are significant or one of the units has stopped charging, the energy loss caused by keeping other units idle becomes greater than the energy gained by harvesting energy from the slowest unit. Upon closer inspection of these cases, a threshold can be detected where the MFC unit becomes no longer beneficial for the system's energy output. The proposed method identifies the slowest MFC unit in the stack and decides whether to keep the unit in the power harvesting process or discard it.

To give the algorithm the ability to discard certain units, the PMS configuration utilizes the SWB parallel switch illustrated in Figure 2.3 to bypass the unit in case the algorithm detects it as "not beneficial". Adding a new switch per each MFC unit would not add a big source of ohmic loss to the system since the current only flows through SWBi switch when the MFC_i unit is being bypassed and not during the normal operation of the system where all the units are connected and functioning. To decide if a unit is beneficial or not, the discarding algorithm needs to measure or estimate the system's energy output in two cases. Firstly, while the slowest unit is connected, and secondly when the unit is disconnected from the system. Since the important goal of the PMS is to increase the total energy output during any given period, the algorithm utilizes average power output comparison instead of energy output comparison to evaluate the performance of the PMS, since if the mean output power is maximized during a certain period then the output energy is maximized during the same period, as well.

For this purpose, the average power output levels of the system with ($\overline{P_a}$) and without ($\overline{P_b}$) the slowest unit are calculated and compared. This comparison determines if disconnecting is beneficial with regard to the mean power output of the system or not. Calculating average power ($\bar{P}$) is based on the energy charged into each C_i capacitor and the time it takes to complete a cycle. Cycle period of the system (Δt_{total}) is defined as:

$$\Delta t_{total} = \Delta t_{cj} + \Delta t_d, \tag{2.8}$$

where j is the slowest unit to finish charging, Δt_{cj} is the time needed by the slowest unit to charge its capacitor from V_{Lj} to V_{Hj} and Δt_d is the time it takes the system to discharge all the C_i capacitors from their higher threshold to the lower threshold. The power calculations are shown in equations (2.9) to (2.11):

$$E_{total} = \sum_{i=1}^{m} 0.5\ C_i \left({V_{Hi}}^2 - {V_{Li}}^2\right) \tag{2.9}$$

$$\overline{P_a} = \frac{E_{total}}{\Delta t_{total}} \tag{2.10}$$

$$\overline{P_b} = \frac{E_{total} - E_j}{\Delta t_{total-new}} \tag{2.11}$$

where m is the number of connected units, Δt_{total} is the system's cycle period with the slowest unit connected, $\Delta t_{total\text{-}new}$ is the system's cycle period with the slowest unit being discarded from the system, and j is the index of the slowest unit. The weakest unit is discarded whenever the following condition is satisfied:

$$\overline{P_a} < \overline{P_b}. \tag{2.12}$$

Regardless of the total number of MFCs while evaluating $\overline{P_a}$ and $\overline{P_b}$ values, only the connected units are considered towards total energy or Δt_{total}. As an example, in a stack of 10 MFC

units, if MFC_1 was discarded recently, in the next cycles, $\overline{P_a}$ and $\overline{P_b}$ values are calculated without MFC_1 and the slowest unit is determined among the remaining nine units.

Although discarding a unit would decrease the harvested energy over one cycle, the reduced cycle period can increase the system's average power output and therefore, total energy harvested over a long period.

By disconnecting the slowest unit, the algorithm attempts to increase the whole system's performance and, meanwhile, give the disconnected unit time to recover and potentially increase its power production once reconnected. The algorithm is allowed to disconnect "non-beneficial" units as long as the remaining units can sustain the power harvesting process, i.e. the supercapacitor's voltage is high enough to activate the semi-conductors in the boost converter. Given the average voltage of the MFC units available for this study and the topology of the proposed method, the minimum number of MFCs that can supply the forward voltage of the boost converter is two MFC units. This means, regardless of the total number of MFC units, the algorithm is allowed to disconnect as many units as necessary, as long as there are two units available for power harvesting.

After disconnecting a unit, at specific intervals (RT), the algorithm keeps calculating the potential cycle energy output of the disconnected unit(s) based on V_{OCi} and existing C_i capacity and reconnects them if their energy is larger than the average cycle energy of the existing units. The effect of the newly reconnected is not clear beforehand, thus the power comparison is performed once again after reconnecting to see if this reconnection is beneficial for the system or not. The flowchart of this algorithm is depicted in Figure 2.4.

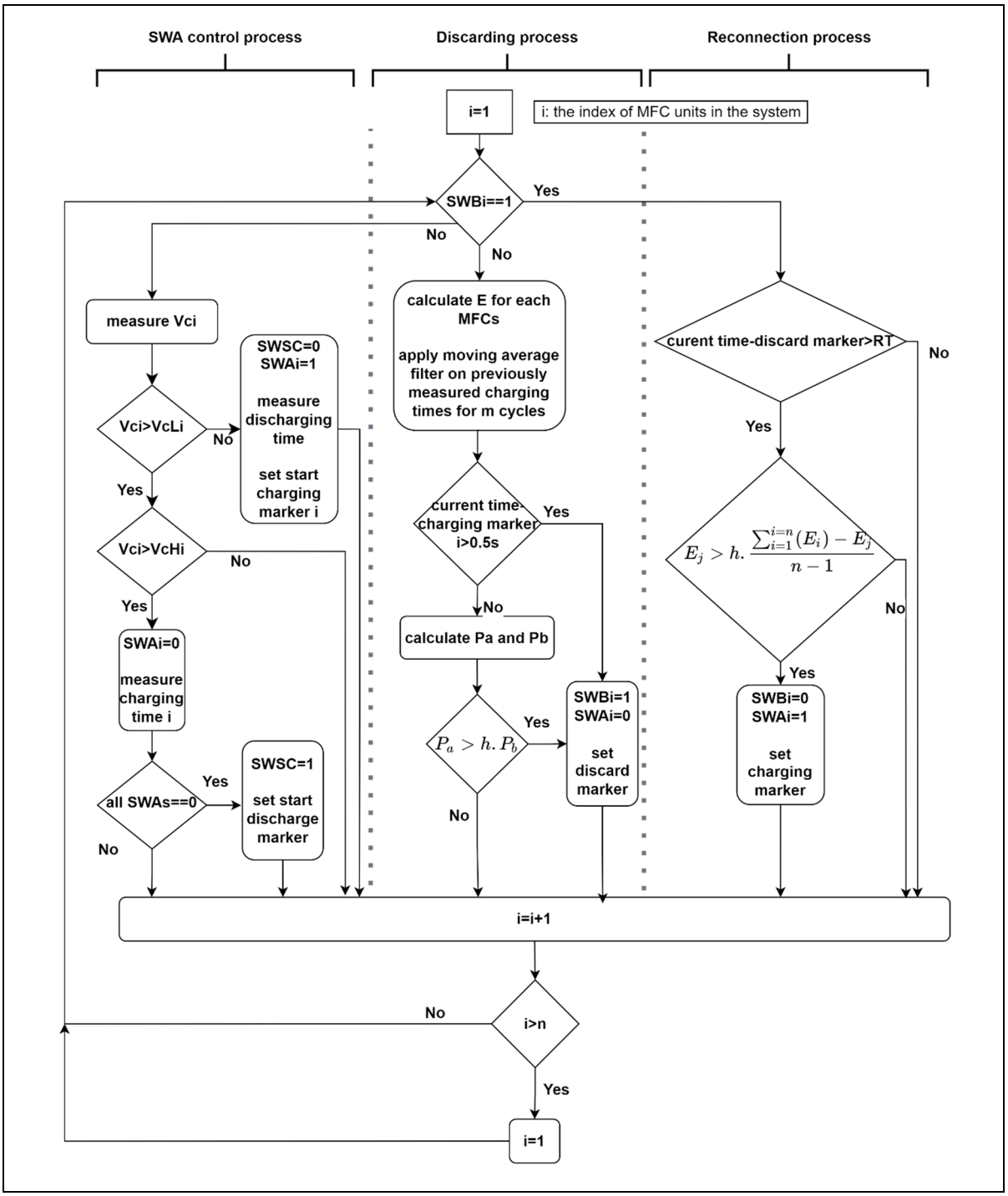

Figure 2.4 Flow chart of the proposed algorithm

2.5 Limits of the proposed method

Let us assume that we have a three MFC stack, as presented in Figure 2.3, for which $\Delta t_{c1} > \Delta t_{c2} > \Delta t_{c3}$. When only two units are connected, the time needed for discharging capacitors C_i to the supercapacitor C_{sc} (Δt_d), is longer compared to the case where all three units are connected. This increase in Δt_d affects Δt_{total}, as shown in equation (2.8).

The disconnection of one MFC unit also influences the internal behavior of the connected MFCs. While the system is in the discharge state, MFC reactors are isolated from the rest of the circuit. However, in the meantime, a new equilibrium of charges is taking place inside the reactor. This effect can be simulated using the internal capacitor of the MFC equivalent circuit representation illustrated in Figure 1.4 (Macdonald & Johnson, 2018). Assuming the MFC unit is defined solely by its electrical equivalent model, presented in Figure 1.4, while charging the C_i capacitor, voltage would inevitably be divided between C_i and C_{int}. However, whenever the discharging period (Δt_d) is prolonged, the internal capacitor would discharge through its parallel resistance (R_2) for an extended period and, consequently, the voltage at the internal capacitor will reach a lower value at the end of the discharge period. This unintentional decrease in C_{int} voltage level will increase the charging period (Δt_{ci}) in the next cycle. Indeed, once SWAs are reconnected, the MFCs have to recharge both their internal and external capacitors C_{int} and C_i, respectively. Estimating this increase in charging time beforehand is not possible due to the complex nature of an MFC.

As a result of this chain process, after disconnecting one unit, the discharging period increases, and the charging period for the connected units is prolonged. Hence, it shows that the value of $\overline{P_b}$ calculated in equation (2.11) is not an accurate representation of the power output of the system after discarding one unit. To tackle this problem, attempts were made to re-evaluate the condition mentioned in equation (2.12) right after disconnecting the slowest unit and reconnecting the unit if the condition is not satisfied. However, these attempts caused a chattering problem in the SWB_j switch, repeatedly turning the switch on and off before reaching a steady state, as illustrated in Figure 2.5.

Moreover, while calculating $\overline{P_b}$ in equation (2.11), the energy contribution of the discarded unit is assumed to be zero, however, due to the losses in the SWB of the discarded unit, the energy contribution of this unit should be negative. It should be noted that the same overestimation does not apply to $\overline{P_a}$ calculation in equation (2.10) since the calculation is based on the voltage of the C_i after the loss in SWA_i has happened.

The second issue that this algorithm faces while discarding units is the sensitivity to minor disturbances. Since the condition in equation (2.12) uses only information from one cycle and feeds it to discarding algorithm, temporary disturbances (that happen during one cycle) can negatively affect the performance of the algorithm. Moreover, if one MFC is not able to charge its C_i capacitor, the other units wait indefinitely, and the power extraction will be stopped.

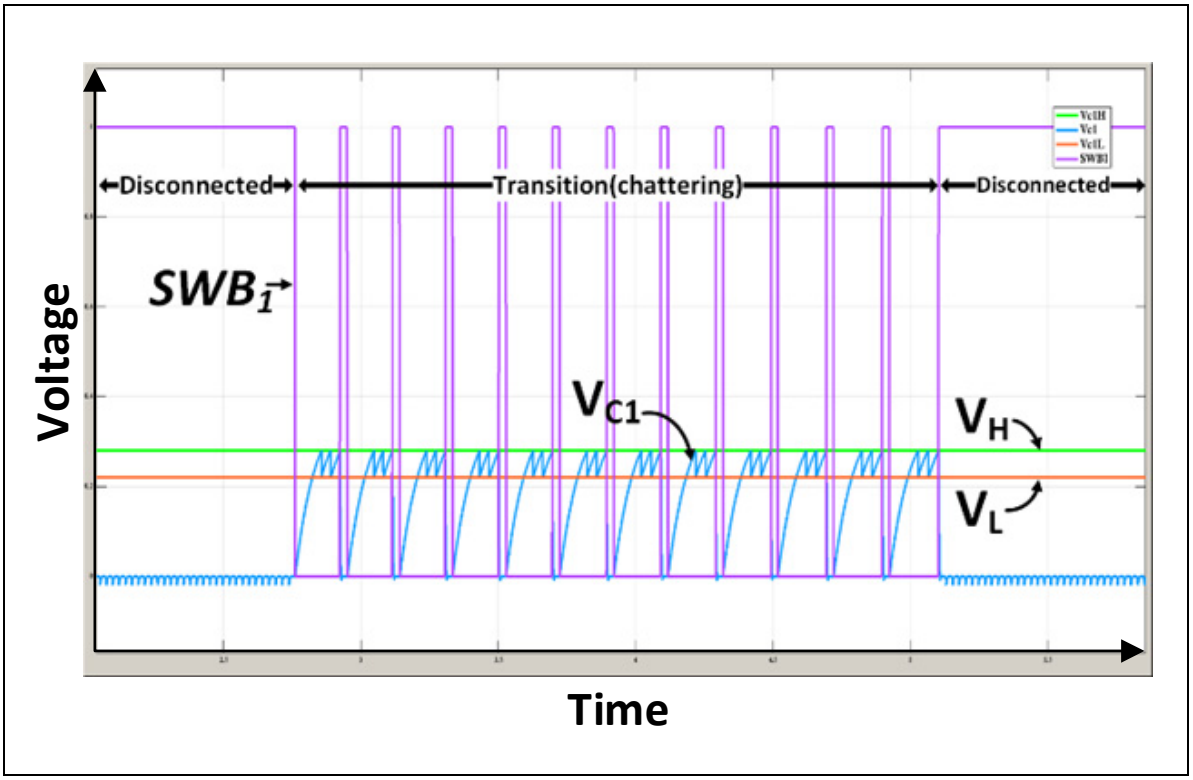

Figure 2.5 Chattering effect seen in SWB switch of the slowest unit (MFC_1)

2.6 Modification of the proposed algorithm

Two control methods are added to the proposed algorithm to tackle the chattering issue. These methods are discussed in sections 2.6.1 through 2.6.3, respectively.

2.6.1 Hysteresis method

The hysteresis method introduces a tolerance margin to the condition used in discarding algorithm, presented in equation (2.12). In this method, the threshold bar, which is used to determine if a unit is beneficial for the system or not, is increased to compensate for the two sources of overestimation in the calculation of the $\overline{P_b}$ value using equation (2.11) and the condition in equation (2.12) can be modified to equation (2.13).

$$h.\overline{P_a} < \overline{P_b} \tag{2.13}$$

where h is the hysteresis coefficient. This parameter is always larger than 1 and it could range from 1 to 4 based on the characteristics of the problem. Figure 2.6 is an example representation of the hysteresis method. It shows the sudden changes in $\overline{P_b}$ and how the extra margin can prevent the chattering problem.

Although this method significantly reduces the occurrence of chattering, usage of margin forces the algorithm to avoid discarding in certain cases. Consequently, while using this method, there is a possibility of small potential energy loss.

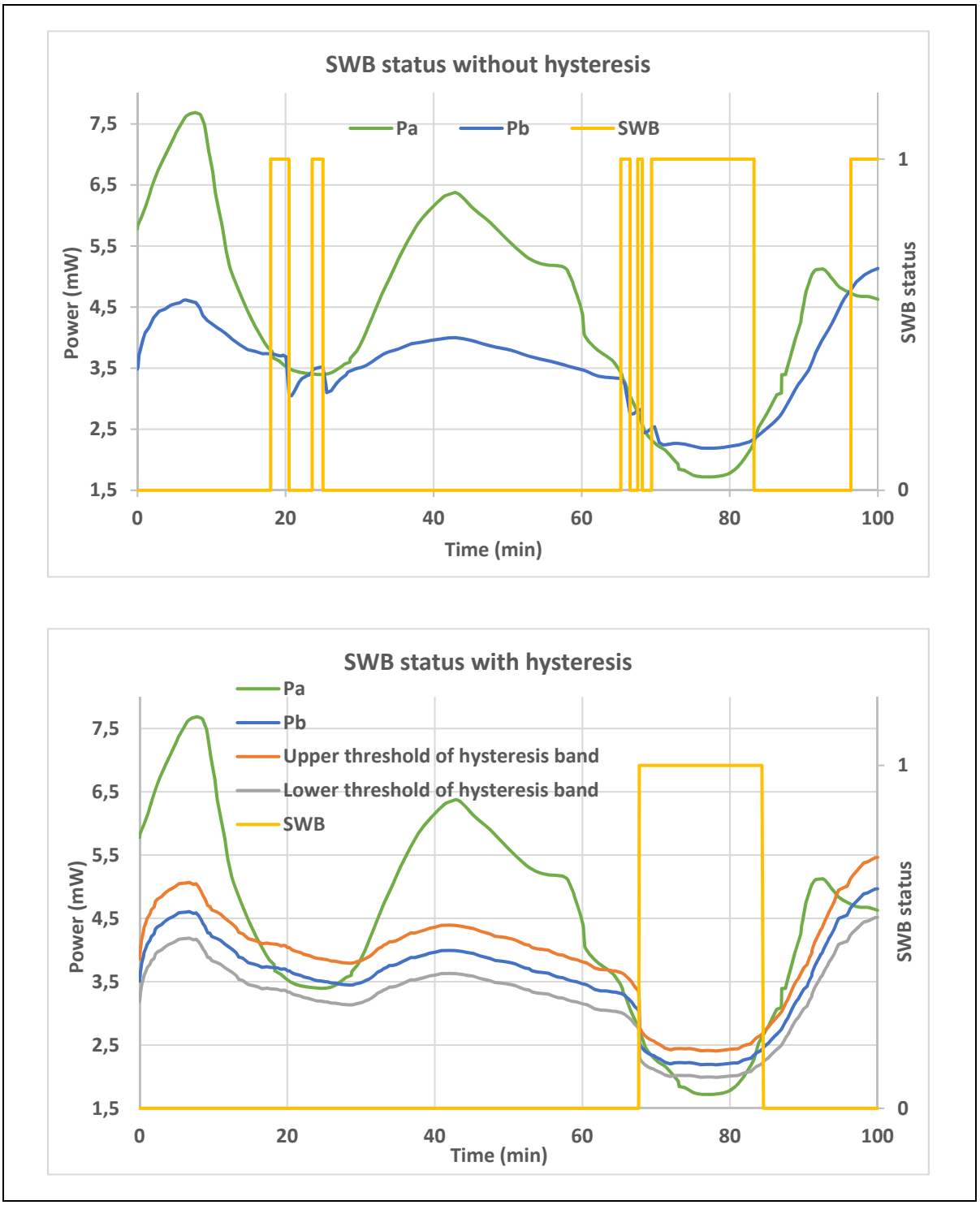

Figure 2.6 Effect of hysteresis method in the prevention of chattering problem

2.6.2 Simple moving average (SMA) method

For the discarding algorithm to depend on one cycle can be misleading, especially when the system is exposed to temporary disturbances. To mitigate the effect of short-lived disturbances and momentary measurement errors, the SMA method would base the decision to discard or reconnect an MFC unit on several (m) cycles rather than one.

This method changes how average power is calculated and replaces equations (2.10) with equation (2.14).

$$\overline{P_a} = \frac{1}{m}\left(\sum_{k=k_0}^{m+k_0} \frac{E_{total_k}}{\Delta t_{total_k}}\right) \tag{2.14}$$

where the SMA method calculates the average power starting from cycle number "k_0" for a total of "*m"* cycles.

Utilization of this method will enable the proposed algorithm to reduce sensitivity to temporary disturbances which last less than "*m"* cycles. The drawback of this method is that it delays the evaluation of equation (2.13) for "*m"* cycles and causes the system to lose a small amount of potential energy before discarding. However, since this method is just averaging the values of "*m"* cycles, the discarding can happen before "*m"* cycles are finished depending on the size of changes. Just like the hysteresis method, if used alone, the SMA method would not solve all the issues in the originally proposed algorithm. Therefore, in this study, both methods were implemented to obtain the best results.

2.6.3 Real-time Charging observation

In case the charge state has begun but one of the MFCs is not able to charge its C_i capacitor in a reasonable period, the power extraction can be hindered or completely stopped. This type of malfunction can be caused by an electrical disconnect in the wire or physical damage to the

MFC reactor itself. The proposed algorithm wouldn't be able to manage such problems since it only checks the charging duration after the charging state is completed, so if the voltage of the C_i capacitor (V_{Ci}) doesn't reach its higher threshold the algorithm cannot detect that the unit *i* is hindering the system. To address this issue, the algorithm needs to observe the charging periods, in real-time, and make sure a unit doesn't take more than a "typical charging period" to charge its C_i capacitor.

2.7 Boost converter

Since this power management system is designed to eventually have real-world applications, the output voltage at the load level should be high and stable enough for typical electronics to function.

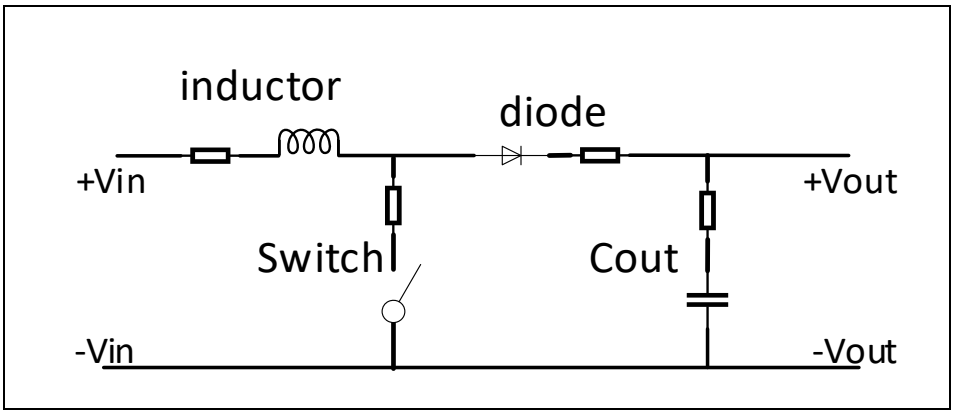

Figure 2.7 Realistic topology of the step-up converter
with all the ohmic losses

The voltage at the supercapacitor level depends on the number of MFCs connected and their open-circuit voltage. Based on the typical values from SAMFC units in our lab, the supercapacitor voltage level with 4 MFCs connected in the system would be varying between 0.3V to 1.5V. To increase this voltage, a conventional boost converter is utilized (shown in Figure 2.7 as a part of the whole topology). This form of converter has been tested in similar configurations before, where the input voltage of the converter was in the order of a few hundred millivolts (Mukherjee et al., 2022; Nguyen et al., 2019). Given the low input voltage

and power of the converter, to keep the efficiency of the boost converter above 90%, the duty cycle should be limited to the 0.1-0.8 range, based on the data presented in Figure 2.8. The relation between the boost converter duty cycle and the voltage boost ratio is shown in equation (2.15).

$$\frac{V_{out}}{V_{in}} = \frac{1}{1-D} \tag{2.15}$$

Based on equation (2.15), limiting the duty cycle to 10%-80% will limit the boost ratio to 1.1 to 5. The problem with having a limited boost ratio is that it would be practically impossible to supply a single output voltage given the vast range of input voltage.

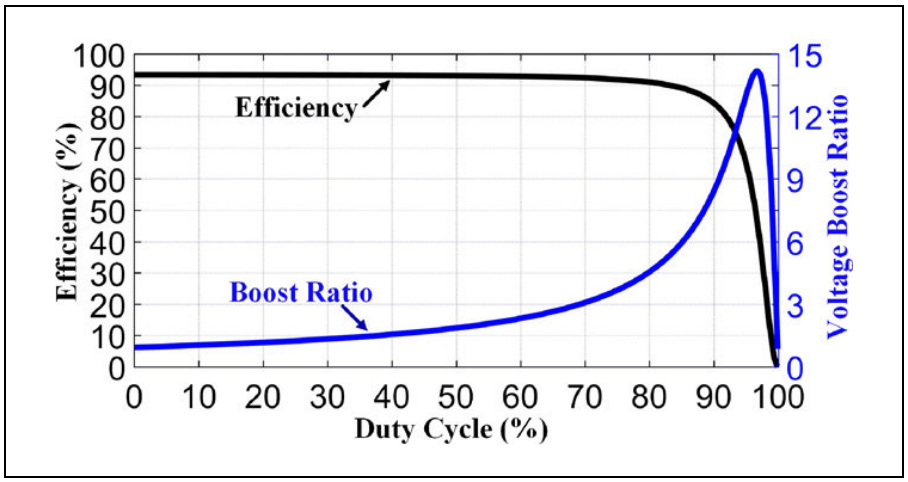

Figure 2.8 Efficiency and boost ratio of the boost converter
as a function of the duty cycle
Taken from Nguyen et al. (2019)

It is possible to have two reference voltage levels in the output based on the magnitude of the input voltage. For example, in a telemetry application, while the output voltage of the converter is set to a lower voltage level the microcontroller (load) can do essential tasks like taking high priority measurements and when the output voltage level of the converter is higher the microcontroller can address other tasks like taking lower priority measurements or sending the logged data.

To stabilize the voltage, a PI controller is used to control the duty cycle of the boost controller. The derivative term of the controller can be very useful in predicting the changes in the input voltage and can potentially reduce the settling time. However, due to the fluctuating nature of converter input voltage (V_{SC}), using the derivative term can cause ripples in the duty cycle and converter output voltage.

In conclusion, this chapter discusses the fundamental idea of the proposed PMS, its drawbacks, and the changes made to enhance its functionality. This chapter also covers the specifics of the voltage boosting and regulation as well as the logic and calculations linked to the Discarding algorithm, which determines when we should connect or disconnect MFC units.

CHAPTER 3

EXPERIMENTAL DATA ACQUISITION AND PARAMETER ESTIMATION

The objective of this chapter is to estimate and simulate the behavior of the stack of MFCs and provide a test case to verify the performance and functionality of the proposed algorithms in CHAPTER 2.

MFC units are not steady sources of power, their output voltage and power are heavily dependent on the internal conditions of the reactor and the external environment surrounding the MFC. This kind of volatility can cause unidentical behavior from one MFC unit to another and challenge the PMS algorithm. To evaluate the effectiveness of the PMS algorithm, realistic MFC data was provided as an input for the PMS algorithm, and the power delivered at the load level was observed to determine the efficiency and functionality of the PMS system. The PMS system comprises the charge pump configuration, the algorithm, and the boost converter.

This chapter will cover the experimental process that we followed to obtain real-world data, and two parameter estimation processes based on experimental data.

3.1 Internal parameter estimation

The first step after developing an algorithm is to validate its functionality with regard to the expected input parameters. In the case of this algorithm, the input of the algorithm is the output voltage of the MFC unit (V_{MFC}). In the simulation, based on the EEC model presented in Figure 1.4, this value is dependent on the internal parameters of the MFC electrical equivalent circuit (V_{OC}, R_1, R_2, and C_{int}). Although in the simulation these internal elements have values and are necessary to recreate the dynamic behavior of the MFC, a real MFC reactor is not made of capacitors and resistors, so these values cannot be physically seen or measured. The only electrical parameter that we have access to is the MFC output voltage and if the EEC is reasonably accurate, these internal parameters of the EEC of the MFC can be calculated with

acceptable accuracy. In sections 3.1.2 through 3.1.4, the process of measuring V_{MFC} and how to determine the internal parameters of the MFC EEC is discussed in detail.

3.1.1 MFCs used in experimental measurement

In the current study, the experimental data acquisitions are done using the four single chamber air-cathode MFCs. These MFC were developed in the GRÉPCI research group during the summer of 2017 and was maintained and produced power until the end of 2021. Although the design of these MFCs is out of the scope of this study, the material, structure, and maintenance of them are explained briefly in this section. Some of the details regarding the size and materials used in the MFCs are taken from (Osiris, 2017).

Each reactor had a 3D printed plastic frame, measuring 21cm×12cm×12cm, that held all the components together. Each side of the reactor was covered by a 21cm×8.9cm carbon paper which had manganese wires interlaced in them acting as the reduction catalyst. The carbon paper sheets were protruding from the top of the reactor giving the user access to the cathode terminal. For the anode material, 18cm×8cm carbon felt (one for each side) was used which has high porosity while having good electrical conductance (1.2Ω/cm). These carbon-felt sheets were installed inside the reactor parallel to the cathode. The cathode and the anode were separated by two polyester membranes each with a thickness of 1.5cm. A titanium rod measuring 24cm was inserted vertically into each carbon felt sheet to give them mechanical strength, decrease their ohmic resistance, and protrude out of the top of the reactor to give the user access to the anode terminal. The top cover of the reactor was screwed to the plastic frame and sealed with silicon to prevent leaking. The top of the MFC was connected to a 125ml reservoir, this reservoir is the only way to access the inside of the reactor and it's used to add water, organic material, or electrolytes to the substrate and make sure that the bacteria are not exposed to oxygen.

The substrate of the MFCs was comprised of equal parts humus and peat moss mixed with enough water to bring the mixture to a mud-like consistency. Although this substrate had a lot

of organic material for the bacteria to degrade, a sugary solution (Lee, Salerno, & Rittmann, 2008) was also provided in a fed-batch process to boost and maintain the substrate COD (chemical oxygen demand) for prolonged periods of time. A 125ml sugary solution consisted of 800mg sugar, 100ml water, and a 25ml buffer solution. The basic buffer solution itself was made of 1L of water, 21.7gr of K_2HPO_4, and 33gr of $Na_2HPO_4.7H_2O$.

3.1.2 Experimental data acquisition

The data acquisition procedure was developed to maximize the information that can be obtained from V_{MFC} measurement later. This means that the value of MFC voltage was measured while the MFC was disconnected from load, and while it was under load to capture the dynamics of the MFC.

Since there were four MFCs available to use in the lab, we chose to have four MFCs in the simulation. The data acquisition experimental setup was made up of the four available MFC units, four mechanical switches, *LabJack U3-LV*, LabJack MATLAB interface, and four identical resistors. The LabJack device was used as a voltage measurement device and was connected to the MFCs in parallel.

The measurement begins after the MFC units were open circuit (the series mechanical switch was open) for more than 45 minutes to ensure that $V_{MFC} \approx V_{OC}$. Then, the switches are manually closed and the LabJack device continues to measure V_{MFC} for 15 minutes when the measurements stop. During the measurements, it was observed that a minimum period of 15 minutes after closing the switch would suffice to capture the transient state of the MFCs as depicted in Figure 3.1. The changes seen 10-15 minutes after closing the switches have a gentle linear slope and can be mostly associated with the changes in V_{OC} caused by the consumption of substrate material in the reactor. Therefore, only measuring 15 minutes after closing the switch would suffice to include the transient state of the MFCs. Moreover, during short measurements (in the order of a few minutes) the changes in V_{OC} can be ignored since typically V_{OC} changes 2%-10% per hour, based on the observations in the lab. The value of the

connected load (resistor) to each MFC during the measurement was 150Ω±5%, which is in the range of optimal external resistance for this specific group of MFCs.

These measurements were taken in a variety of internal and ambient conditions to better represent the real-world conditions. The measurements were carried out in the following five categories:

1. Duration: 24h, period start time: right after feeding MFCs with the sugary solution (transient condition),
2. Duration: 10 days, period start time: one day after feeding (high COD),
3. Duration: 2 days, period start time: 11 days after feeding (Low COD, Low water level),
4. Duration: 2 days, period start time: 14 days after feeding and 1 day after filing the MFCs with only tap water (Low COD, High water level),
5. Duration: 1 hour, period start time: 24h after feeding and 30 minutes after the temperature-controlled chamber has settled on the new temperature (high COD, variable temperature).

MFCs were batch fed by the sugary solution, which consisted of 700mg sugar and 20ml of basic buffer solution for each 100ml of water. During the feeding process, the MFC reactor was completely filled with this solution. The basic buffer solution was added to keep the pH of the MFC reactor neutral while the sugar is being degraded. The buffer solution consists of 21.7gr of dipotassium hydrogen phosphate (K_2HPO_4), and 33gr of disodium hydrogen phosphate heptahydrate ($Na_2HPO_4.7H_2O$) for each liter of water.

Two full cycles of categories 1-4 were recorded during the measurements. Category 5 was measured at three ambient temperatures (23°C, 27°C, and 37°C). In total, approximately 75 sets of measurements were taken from all categories in the following chronological order: 1→2→3→4→1→2→3→4→5. Each set of measurements (data point) included four V_{MFC} values.

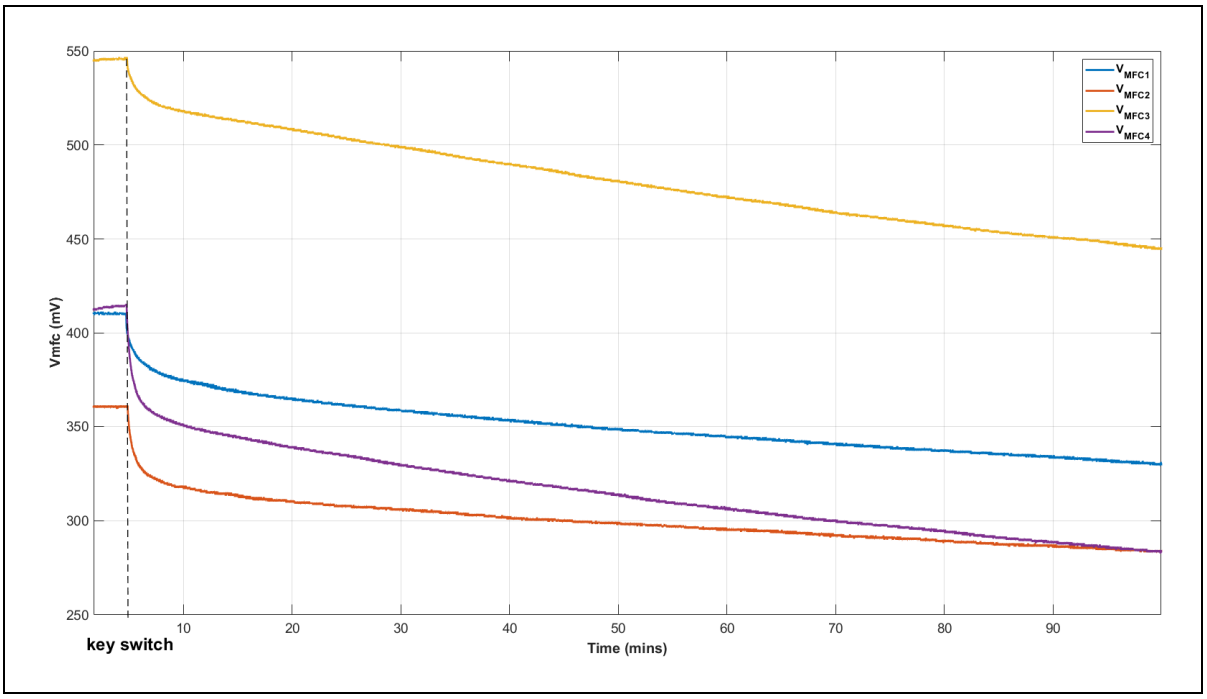

Figure 3.1 MFC output voltages measured for approximately 100 minutes

3.1.3 Analytical approach

In this section, the measurement data obtained from the experiments described in section 3.1.2 is going to be used to identify the internal elements of the electrical equivalent model of the MFC unit. Since there are four internal parameters, at least four measurements of the V_{MFC} at specific points were necessary to give us four linearly independent equations. Each of these points is explained in the steps below.

Step one: The voltage acquisition of V_{MFC} by the data acquisition board starts in this step, which will indicate V_{OC} later in our calculations since the units were open-circuit for at least 45 minutes prior to the measurement.

Step two: At $t = t_0$ the mechanical switch closes and connects the resistive load to the MFC unit. At $t = t_0^+$ we can see a sudden drop in voltage which is caused by the ohmic loss rather than the dynamic behavior of the MFC (Figure 3.2a). This drop can be justified in the

equivalent circuit only by the R_1 resistor since the C_{int} is assumed to be empty and acting as a short circuit at t_0^+. The voltage reading at the dip of this sudden drop would be marked as V_0, as illustrated in Figure 3.2a. The voltage reading right before closing the switch would indicate the V_{OC} value at that point. By having V_{OC} and V_0 values we can calculate the value of R_1 using equation (3.1).

$$R_1 = \left(\frac{V_{OC}}{V_0} - 1\right).R_{ext} \tag{3.1}$$

Where R_{ext} is the external load value.

Step three: After the sharp voltage drop, the voltage is going to drop exponentially even further, justified by circuit time constant and dynamic behavior (modeled by a capacitor in the electrical equivalent model), until reaching a steady state, the voltage reading at this point would be marked as $[t_\infty, V_\infty]$. Having V_∞, V_{OC}, and R_1 values ready and assuming the C_{int} is fully charged at t_∞, we can calculate the value of R_2 using equation (3.2).

$$R_2 = \left(\frac{V_{OC}}{V_\infty} - 1\right).R_{ext} - R_1 \tag{3.2}$$

Step four: Between t_0 and t_∞, the arbitrary point $[t_1, V_1]$ is selected such that $|t_\infty - t_1| > |t_0 - t_1|$. Then point $[t_2, V_2]$ is also chosen from measured data where $t_2 - t_1 = t_1 - t_0$. Assuming internal capacitance voltage (V_{Cint}) is zero at t_0, V_{Cint} as a function of time and V_{MFC} at t_∞ can be calculated from equations (3.3) and (3.4):

$$\begin{aligned} V_c(t) &= V_c(\infty) + \left(V_{C_{int}}(t_0) - V_c(\infty)\right).e^{-t/\tau} \\ &= V_c(\infty)\left(1 - e^{-t/\tau}\right), \end{aligned} \tag{3.3}$$

$$V_{MFC}(\infty) = V_{OC} - V_{R_1}(\infty) - V_c(\infty), \tag{3.4}$$

where $V_c(\infty) = \frac{V_{OC} \cdot R_2}{R_1+R_2+R_{ext}}$, and $V_{R_1}(\infty) = \frac{R_1 \cdot V_{OC}}{R_1+R_2+R_{ext}}$. The voltage of the internal capacitor at t_∞ can be calculated based on equation(3.3).

$$V_{MFC}(\infty) = V_{OC} - \frac{R_1 V_{OC}}{R_1 + R_2 + R_{ext}} - \frac{R_2 V_{OC}}{R_1 + R_2 + R_{ext}} \tag{3.5}$$

$$\begin{cases} V_{MFC1} = V_{OC} - \frac{R_1 V_{OC}}{R_1 + R_2 + R_{ext}} - V_{cint}(t_1) = V_{OC}\left(\frac{R_2 + R_{ext}}{R_1 + R_2 + R_{ext}}\right) - V_{cint}(\infty)\left(1 - e^{-\frac{t_1}{\tau}}\right) \\ V_{MFC2} = V_{OC} - \frac{R_1 V_{OC}}{R_1 + R_2 + R_{ext}} - V_{cint}(t_2) = V_{OC}\left(\frac{R_2 + R_{ext}}{R_1 + R_2 + R_{ext}}\right) - V_{cint}(\infty)\left(1 - e^{-\frac{2t_1}{\tau}}\right) \end{cases} \tag{3.6}$$

In the system of equation (3.6), let's assume $k = V_{OC}\left(\frac{R_2+R_{ext}}{R_1+R_2+R_{ext}}\right)$, $x = e^{-t_1/\tau}$, and $x^2 = e^{-2t/\tau}$. This will change the system of equation as follows:

$$\begin{cases} V_{MFC1} = k - V_c(\infty)(1 - x) \\ V_{MFC2} = k - V_c(\infty)(1 - x^2) \end{cases}. \tag{3.7}$$

Solving the system of equations for *x*, and substituting the value of τ from equation (3.8), the value of C_{int} can be calculated by equation (3.9).

$$\tau = \frac{C_{int} \cdot R_2}{1 + \frac{R_2}{R_1 + R_{ext}}} \tag{3.8}$$

$$C_{int} = \frac{\tau \cdot (R_1 + R_2 + R_{ext})}{R_2 \cdot (R_1 + R_{ext})} \tag{3.9}$$

Since this analytical method is heavily dependent on certain points in the measurement, any kind of noise or different behavior during those specific moments would make it impossible to use this method. For example, one frequent different behavior is the voltage drop mentioned in *step two*. An example of this effect is shown in Figure 3.2 in two different MFC units in different conditions.

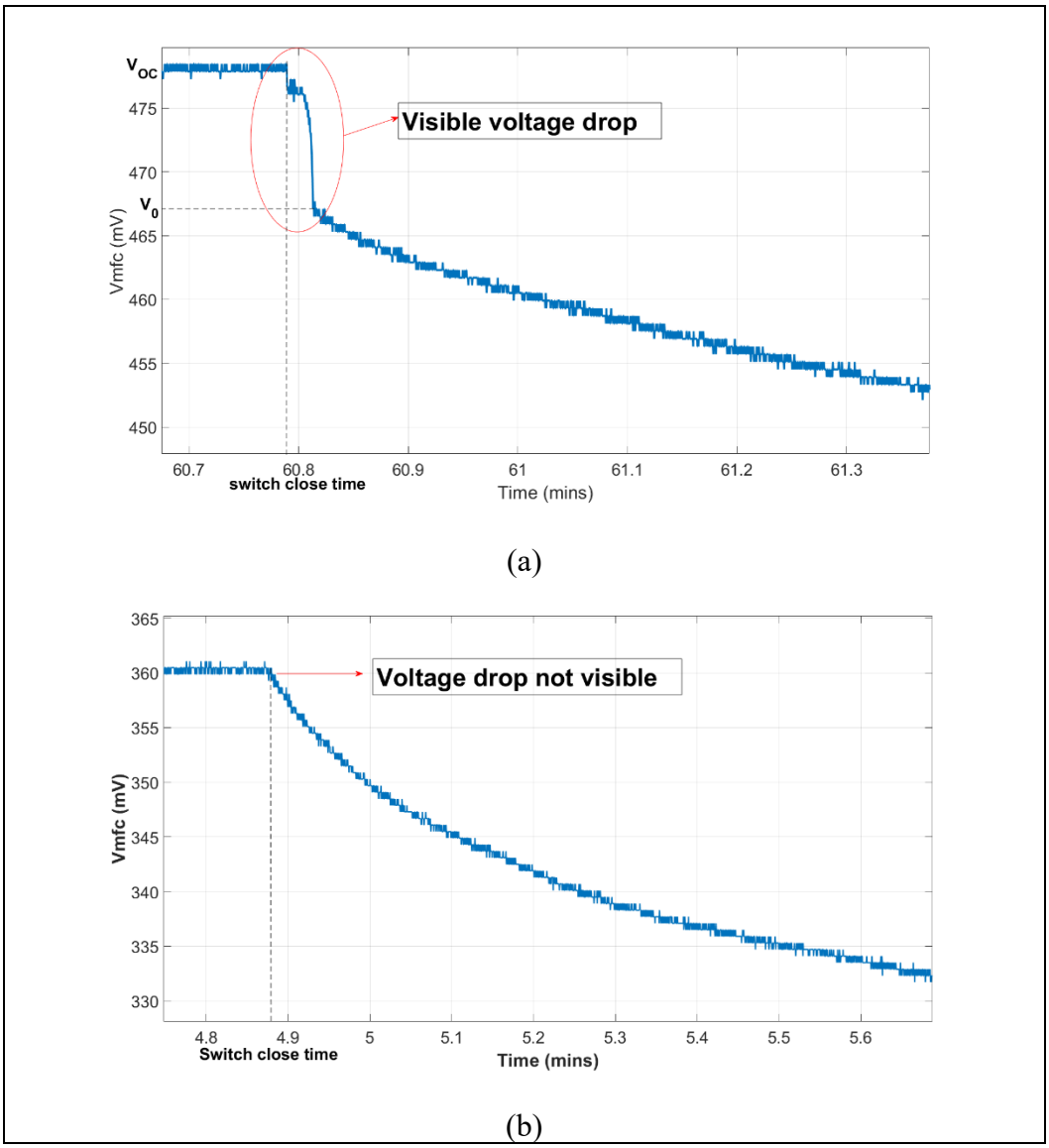

Figure 3.2 Measurements showing voltage drop after connecting the load to the MFC: a) a steep voltage drop can be observed lasting a few seconds b) no visible steep voltage drop can be observed

3.1.4 Optimization approach

To reduce the effect of noise, we can use an offline identification algorithm that estimates the internal parameters of the EEC based on the behavior during a certain period rather than specific points. To do so, the parameter estimation problem is converted into a multivariable minimum mean square error (MMSE) optimization problem with bound constraints. The

variables are the internal parameters of the EEC and the cost function is the mean square error (MSE) between measured and estimated V_{MFC} values. The measured V_{MFC} was provided by the data gathered in section 3.1.2.

The bound constraints (ub, lb) and initial values (x_0) are provided based on typical values from the literature, the exact values are presented in Table 3.1. The optimization was done in MATLAB using *fmincon* function from the optimization toolbox since its able to solve both linear and nonlinear constrained optimization problems.

Table 3.1 The initial values, boundary constraints of each variable in the optimization routine

Variables	Initial value (x_0)	Lower bound (lb)	Upper bound (ub)
V_{OC} (V)	0.45	0.1	0.8
R_1 (Ω)	7	0.2	50
R_2 (Ω)	10	1.0	200
C_{int} (F)	0.7	0.0001	20

The results of this method were then rated by R-Squared (R^2) which measures how well our model fits the actual data; the greater the R-squared, the better the control of the model over the result (Zouggari Ben El Khyat, 2022). Out of more than 100 measurements only 12 of the 75×4 data points (since there are four MFCs in each measurement), had R^2<95%. The data points with very low R^2 values had extreme visible noise or other disturbances during the measurement.

3.2 Preparing test case for simulation

In this section, the goal is to stich the internal parameter values estimated in the previous section in a way that they replicate the real-world experience so it can be fed to the simulations and test its performance. To see the full effect of each variation of EEC internal parameters in the simulation, it is important to let the MFCs reach their steady state between each variation of EEC internal parameters. It was observed that after any changes to the EEC internal parameters, the V_{MFC} value takes about 60 seconds to reach a steady state in the simulation. Moreover, due to the computational limits of our PCs, the maximum simulation run-time possible was 1400 seconds. Therefore, we chose to have 21 sets of data points as our test case, these data points had approximately 64s intervals between them. The selected data points were in the same chronological order as the measurements, so since category 1 was measured first, the data points taken from category 1 appeared first in the test case. We also made sure to include at least two data points from each category of measurements. All the data points in the set had R^2 values higher than 95%. From this point forward, this dataset will be called the *first test case* as opposed to the *second test case*, which is explained later in this section.

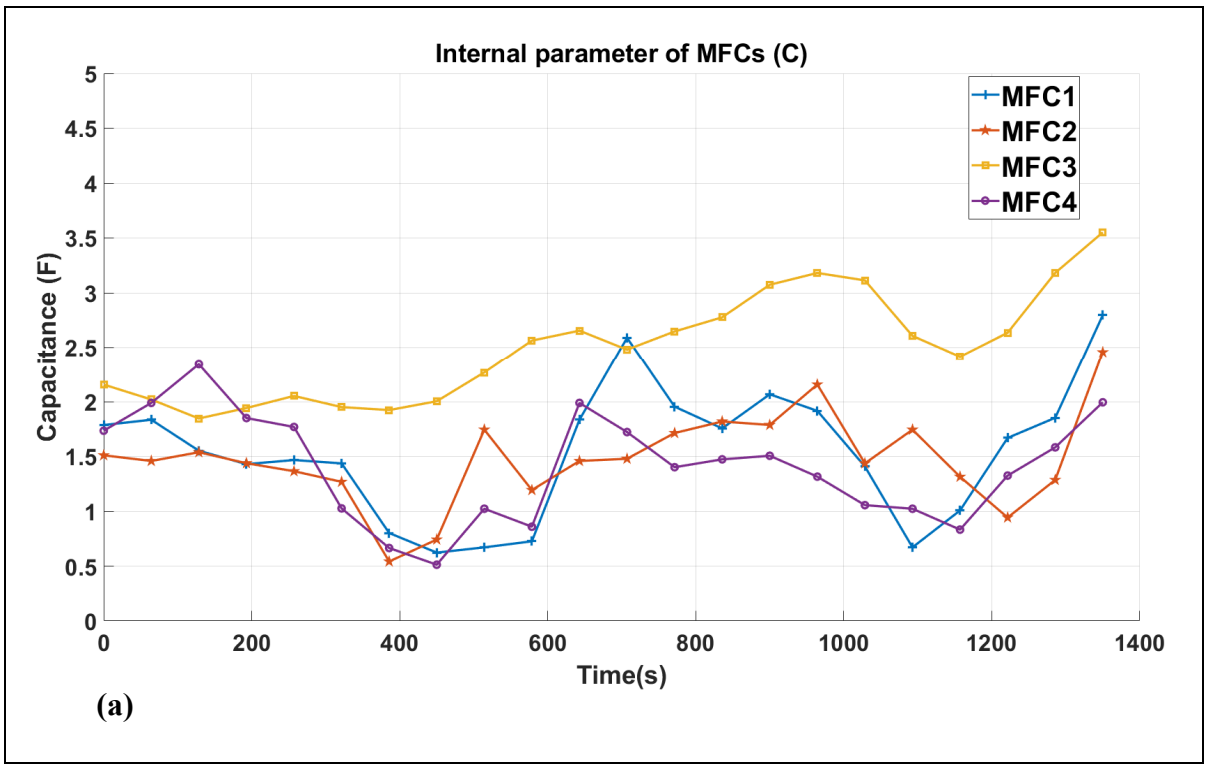

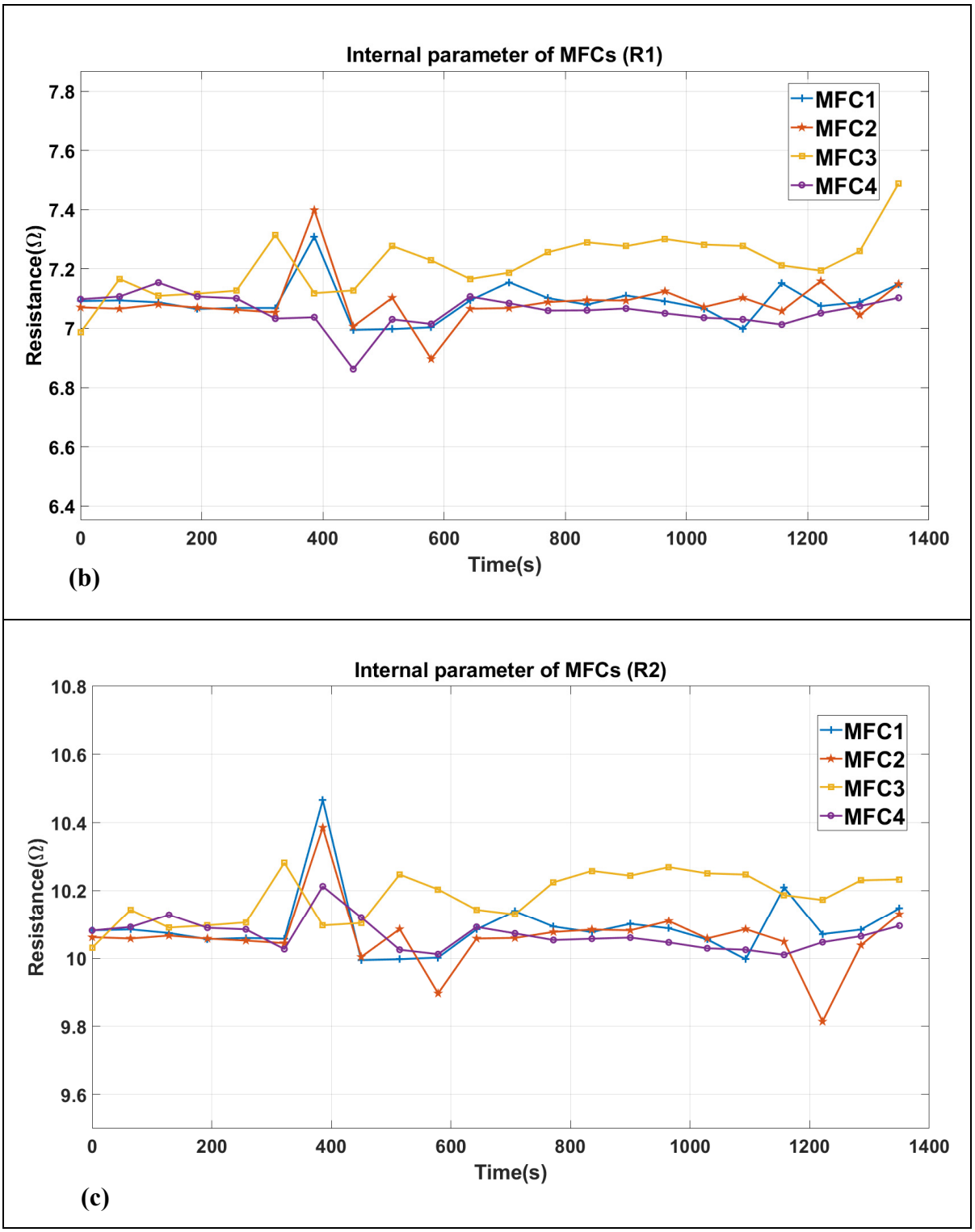

Figure 3.3 Values of internal parameters of electrical equivalent circuit of MFC for test case1: a) C_{int} b) R_1 c) R_2

We also made sure to include at least two data points from each category of measurements. All the data points in the set had R^2 values higher than 95%. From this point forward, this dataset will be called the *first test case* as opposed to the *second test case*, which is explained next.

Since one of the main contributions of this study is that it can extract power even while some MFC units were malfunctioning, there is a need for a *second test case* in which, one of the MFC units has zero output voltage, presenting a malfunction in the MFC or its electrical connection. The second test case is identical to the first test case except for a 64-second period (4.5% of the whole simulation) where only V_{OC3} drops to zero. The V_{oc} values of both test cases are shown in Figure 3.4.

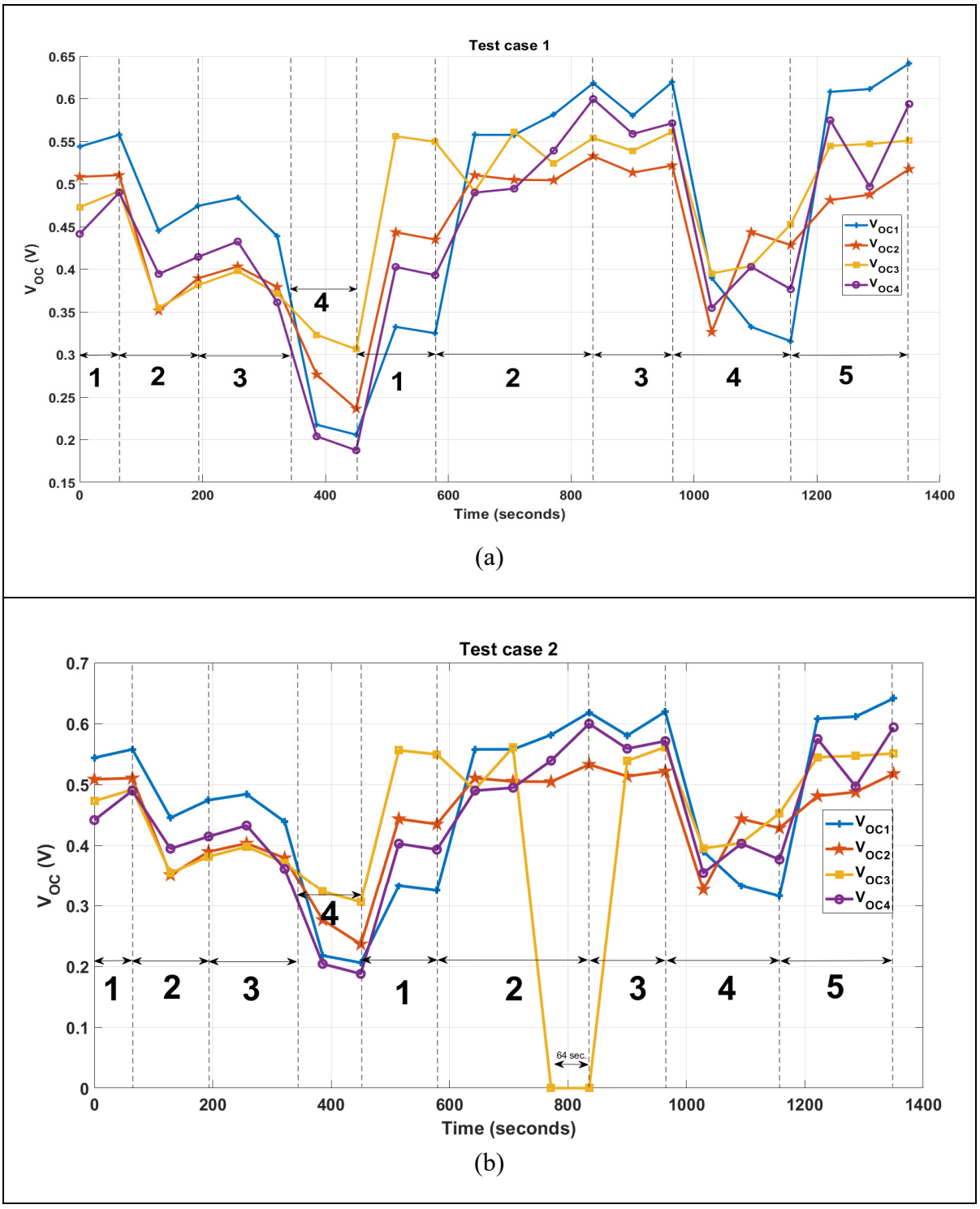

Figure 3.4 V_{OC} values of the: a) first test case and b) second test case

In conclusion, this chapter focuses on the collection and analysis of experimental data. The experimental setup, as well as the duration and circumstances of the experiment are described in detail. Then, using an optimization routine and the raw experimental data, the internal parameters of the MFC electrical equivalent circuit model are identified. After estimating the internal characteristics of the MFC equivalent electrical circuit model under various internal and external conditions, the data is concatenated to create two scenarios of the MFC's characteristics over a certain time period. In this work, these scenarios—also known as test cases—represent a succession of various MFC characteristics in the time domain.

CHAPTER 4

SIMULATION AND RESULTS

For the simulation of the proposed PMS, a stack of four MFCs was selected as shown in Figure 4.1. Each MFC unit is simulated by an equivalent electrical circuit model (as shown in Figure 1.4). The value of each internal element inside the MFC's equivalent electrical circuit model is variable to give us the ability to change their values during the simulation according to the operational conditions. These variable internal elements are illustrated in Figure 4.2.

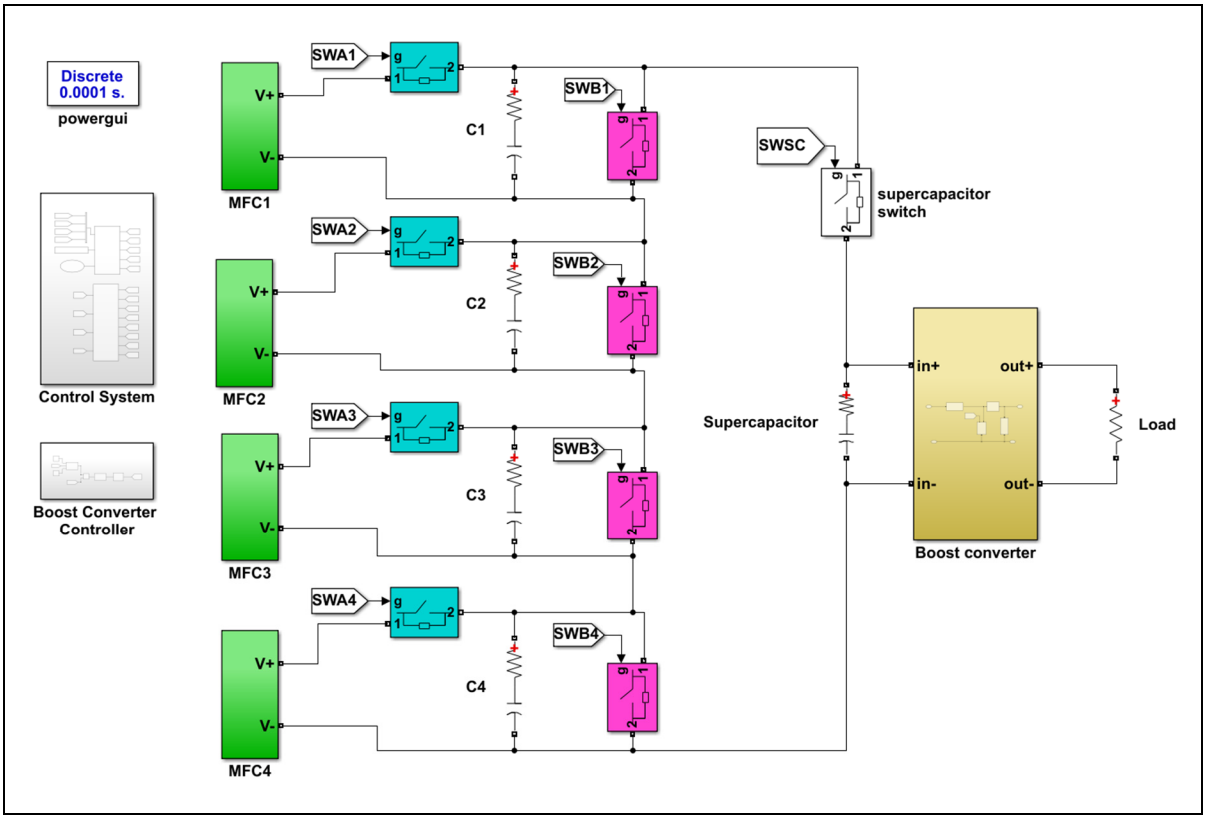

Figure 4.1 The SIMULINK schematic of the PMS

The algorithm is implemented in a MATLAB function, which controls the state of the switches in the system, except boost converter switch. The Boost converter switch (SWBC) is controlled separately by a PI controller (Figure 4.3), which makes the voltage regulation possible.

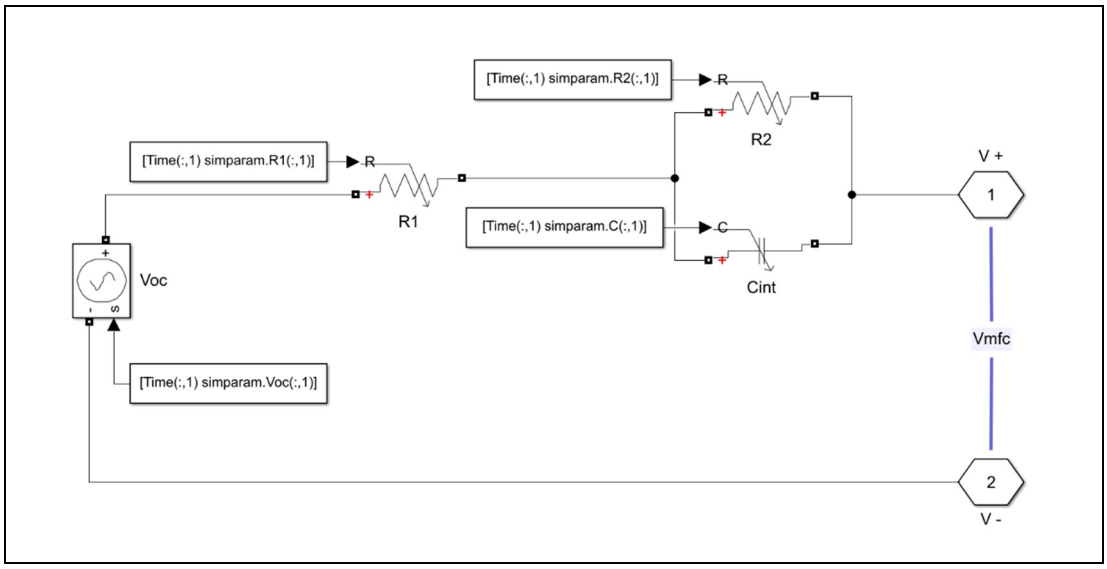

Figure 4.2 Internal elements of an MFC unit in the simulation

The goal of this section is to build a simulation that can verify the functionality of the algorithm proposed in CHAPTER 2 under conditions that are close to real-world experiences and compare the results to a previous study (Nguyen et al., 2019). The test cases used in these simulations are the two datasets presented in section 3.2, based on the estimations and assumptions discussed in section 3.1.4. The test cases provide the values for variable elements at certain points in time (≈64s apart). The values of the elements between these points in time are linearly interpolated to make sure there is a value at each simulation step.

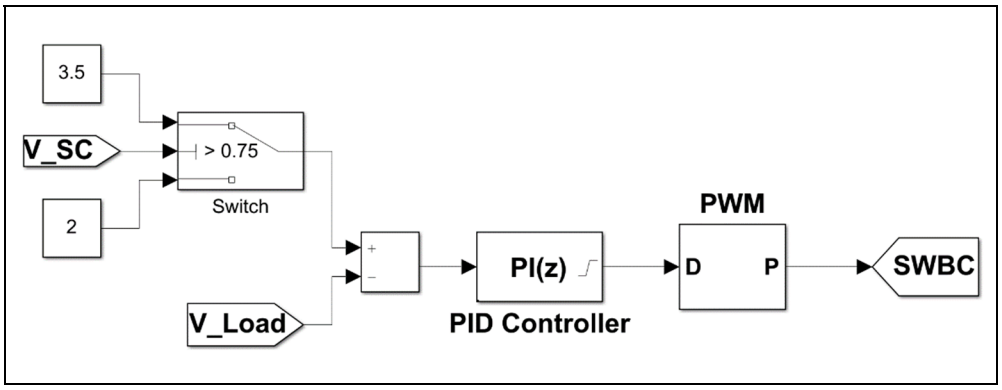

Figure 4.3 Boost converter control unit for voltage regulation

For determining the simulation step size there are two constraints: one is the computational restriction (since to be able to study the long-term performance of the PMS its necessary to run the simulation for as long as possible) and the other is that the simulation step size should be able to match the fastest changes in the system. During the simulations it was observed that the minimum duration of either state of the system (charge or discharge) was about "$7 \times 10^{-4}\ s$". Based on this fact, the simulation step size needed to be small enough so that the simulation has a good resolution of data to act upon. On the other hand, it also needed to be large enough so that running the simulation for more than 1000 seconds doesn't crash the system on which the simulation is running. Considering all the constraints, step size of "$10^{-4}\ s$" was chosen for the simulations.

The exact values of some parameters of the PMS system including algorithm and the circuitry and how to obtain them are going to be discussed in the following sections of this chapter.

4.1 Simulation parameter determination

4.1.1 Circuit elements

Since the power output of this simulation is going to be compared to another study, it is crucial that all the internal elements of the MFCs and the external circuit elements have the same values in the comparison of the two approaches. By doing so, the only aspect in the comparison simulation that changes would be the algorithms and all the other aspects like MFC characteristics, values of circuit elements, converter parameters would be identical between the two approaches, which will ensure the validity of the comparisons.

Table 4.1 Values of the circuit components used in the simulation

Element name(s)		Main value	Parasitic resistance
MFC harvesting elements	**C_i**	3 mF	0.1 Ω
	SWA_i - SWB_i	-	0.4 Ω
	C_s	1 mF	0.3 Ω
Boost converter elements	**L**	0.5 mH	0.6 Ω
	D	V_F = 0.21 V	0.24 Ω
	C_O	2 mF	0.15 Ω
	R_L	5 kΩ	-

The values of the circuit elements presented in Table 4.1 are in accordance to the values mentioned in the study done by Nguyen et al. (2019). The values of the internal elements of the MFCs used in both approaches are the test cases discussed in section 3.2.

4.1.2 Parameters of the proposed algorithm

In the PMS algorithm presented in CHAPTER 2, there are few variables that have a big influence on the functioning of the algorithm, namely *m*, *h*, and *RT*. The formerly presented algorithm is designed as a general harvesting algorithm for stack of MFC units, these parameters can be used as tuning variables to meet the needs of each individual energy harvesting system. The harvesting systems can differ in the number of MFC units in the stack, load, converter type, and voltage levels of the MFCs and therefore, the value for these tuning parameters can be different from one PMS to another.

Table 4.2 Values of mean output power with first test case as input (mW)

Variables		Mean output power (mW)												
		Hysteresis coefficient (h)												
RT	**m**	**1.02**	**1.04**	**1.07**	**1.12**	**1.16**	**1.3**	**1.6**	**2**	**2.2**	**2.5**	**3**	**3.5**	**4**
30	10	1.691	1.709	1.721	1.719	1.723	1.718	1.812	1.817	1.814	1.819	1.817	1.816	1.807
	16	1.691	1.709	1.721	1.719	1.723	1.718	1.812	1.817	1.814	1.819	1.817	1.816	1.807
20	7		1.732							1.814				
	10	1.711	1.731	1.741	1.725	1.743	1.802	1.809	1.815	1.814	1.812	1.819	1.819	1.812
	12		1.731	1.741										
	16		1.73	1.741	1.724		1.801		1.815	1.814	1.812			
	20		1.73						1.815			1.819	1.819	
	50										1.812			
10	10	1.743	1.745	1.739	1.749	1.753	1.808	1.819	1.821	1.821	1.819	1.817	1.817	1.812
	16	1.743	1.745	1.737	1.749	1.753	1.808	1.819	1.821	1.821	1.818	1.817	1.817	1.812
5	10	1.769	1.78	1.759	1.769	1.78	1.812	1.82	1.821	1.821	1.82	1.818	1.815	1.812

In this study the parameters were determined by trial and error in a wide range since it was algorithm's first application. The main objective was to obtain the value that results in the highest output power at load level. The values of *m*, *h*, and *RT* were increased by small increments until a peak and a following dip was observed to verify the pattern. The result of the trial and error is shown in Table 4.2. This table uses a color scale to better illustrate the levels of mean output power and how they compare to each other. The values higher than 50^{th} percentile have a green shade, values below 50^{th} percentile have a red shade, and the value in 50^{th} percentile are white. The darker the shade of green the higher the mean output power value, and the darker the shade of red the lower the mean output power value.

In case of *m*, it can be observed in Table 4.2 that different values do not have a significant impact on the output power. This was expected, since this variable was only introduced to reduce the impact of temporary disturbances including noise in the measurement of V_{MFC} but in this study, the V_{OC} and V_{MFC} values do not have any kind of noise. During the course of this chapter all the presented simulations would assign a value of m=10. Even though the input data in the simulation doesn't have any noise, noise is inevitable in experiments specially since the voltage levels are low and noises can have a significant impact.

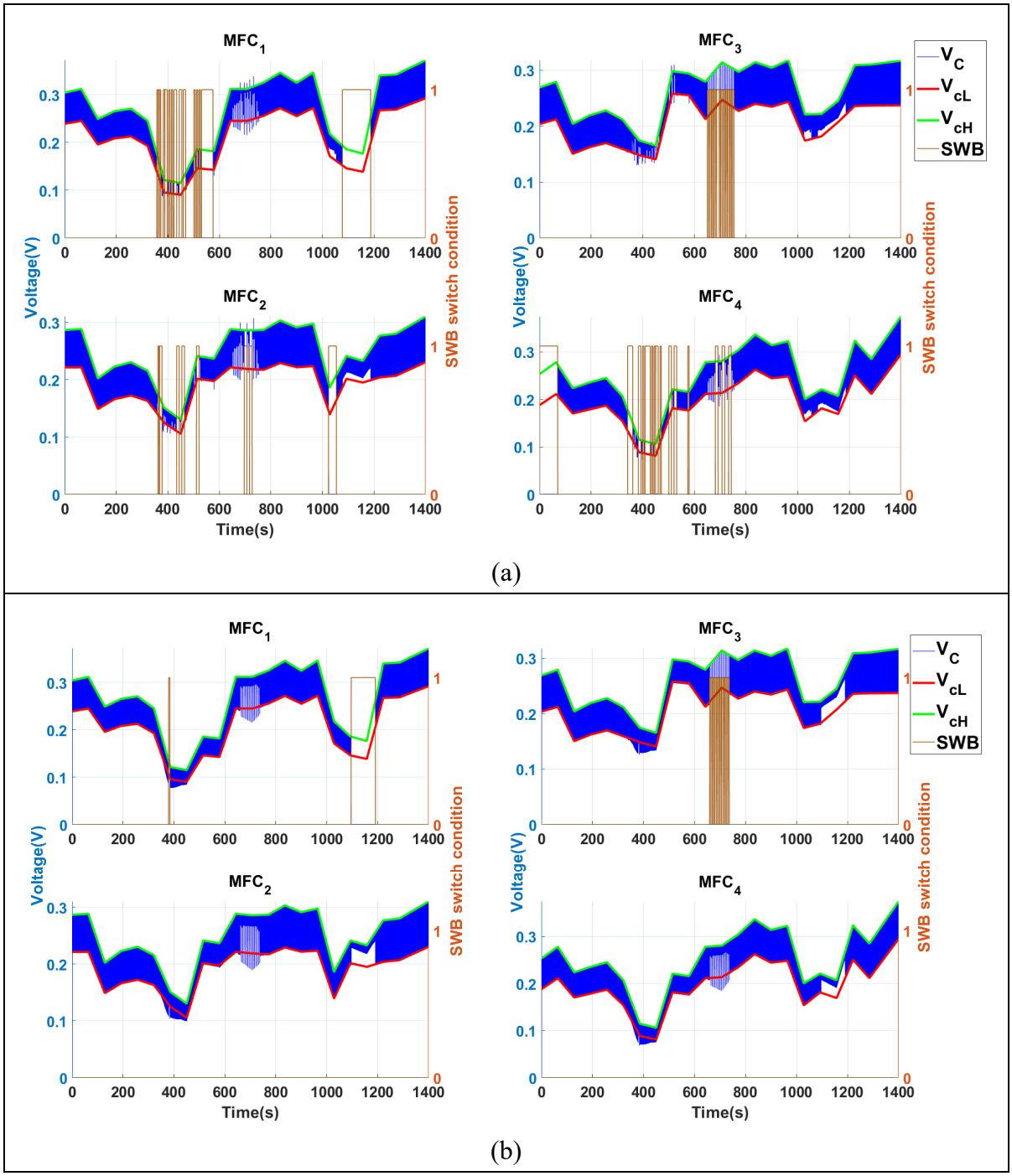

Figure 4.4 V_{Ci} (blue) and SWB_i (brown) of the 4 MFC units for a simulation of 1400s in which the algorithm parameters are set to m=10, RT=5s a) h=1.04 b) h=2

It can be concluded that for higher values of RT, since the discarded unit needs to wait longer to be considered for reconnection, the price of discarding increases. This is due to the fact that,

there are moments where it is beneficial to reconnect a discarded unit, however, the algorithm is still waiting for "*RT* period" to end and this causes potential energy loss. It is also observed in Figure 4.4 that *h* coefficient is acting as a barrier for discarding units, the higher the value of *h* the lower the number of discarding instances during the simulation. Therefore, in simulations with high *RT* value, thus, to yield higher power output, they require higher *h* values to block unnecessary discarding instances. In Figure 4.4, the inconsistencies in the charge and discharge of MFC (blue color) are mainly caused due to the chattering of another unit during the same period. For instance, in Figure 4.4b, while MFC3 is chattering during 650s-720s, other MFCs charge and discharge cycles are disturbed during the same period. This disturbance is why chattering in one MFC is causing potential power loss in the whole MFC stack, and why it should be avoided as much as possible.

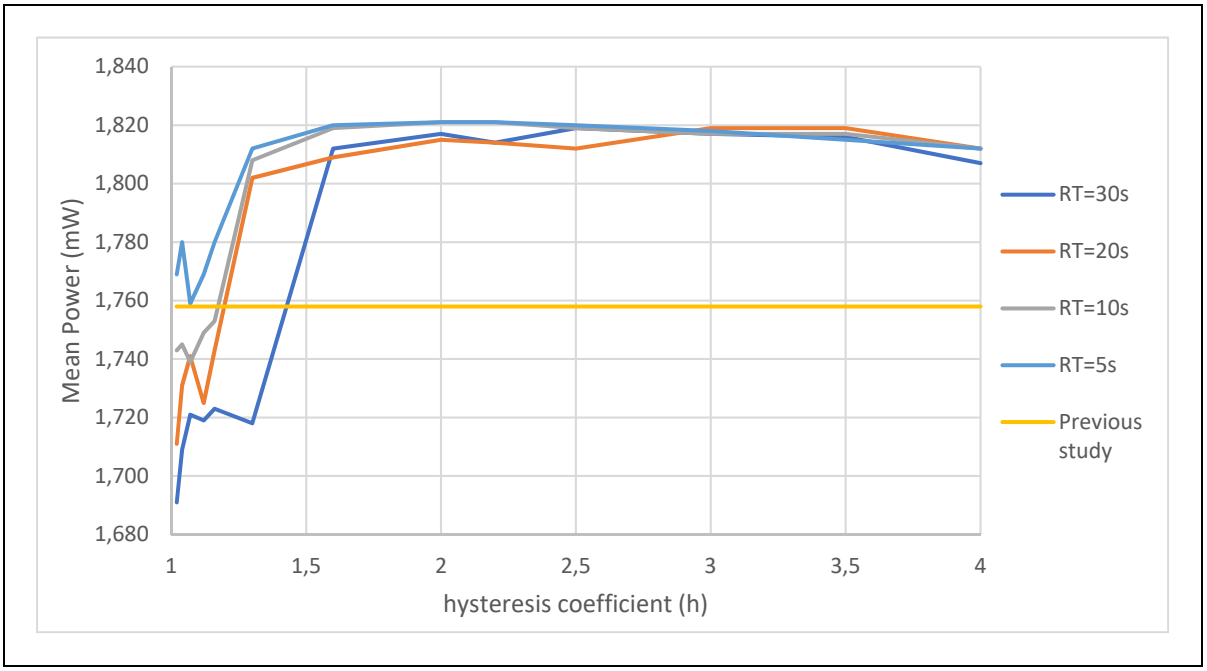

Figure 4.5 Mean power output as a function of *h* for different *RT* values (m=10)

Figure 4.5 illustrates the mean output power of the system as a function of *h* coefficient for different RT values and compares them to the mean power output of the previous study (Nguyen et al., 2019). It is worth noting that the values of EEC internal parameters during these simulations was the first test case in case of the simulations of the proposed method and

previous study. It can be seen from Figure 4.5 that for this test case example, *h* values of 1.5-3.5 result in higher mean power output values, where the peak is at *h*=2 for *RT*=5.

4.1.3 Parameters of boost converter

The parameters of the boost converter have a substantial effect not only in the mean output power at load level but on the harvested energy from the MFCs, as well. These elements determine how efficiently and how fast the supercapacitor is going to be discharged to the load and consequently how fast the C_i capacitors can be discharged to supercapacitor, and in a chain of actions, it affects the energy harvesting rate of MFCs. This underlines the importance of boost converter design based on the source and application.

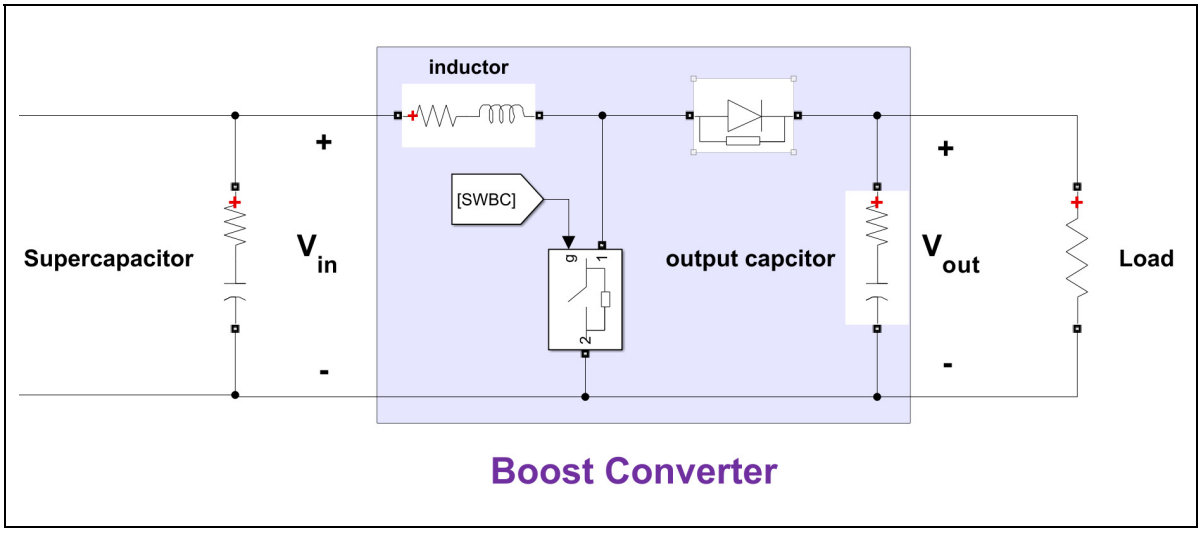

Figure 4.6 The schematic of the step-up converter in the Simulink

The design of the boost converter starts with determining the switching frequency (F_{SW}), which has a considerable effect on the design of other elements of the converter. This parameter affects the gate signal frequency of the SWBC, shown in Figure 4.6. The previous study (Nguyen et al., 2019) didn't have a fixed switching frequency and managed the converter switch each time the controller function was called. Although it might work for some application it makes it harder to optimally tune the elements of the converter. In the proposed

PMS, we use a fixed switching frequency based on its computational burden for the simulation. since higher frequencies of the PWM are computationally more expensive, we have decided to choose a low frequency of 500Hz for the boost converter switch. Nevertheless, in experimental tests where computational cost is not an issue, it is advised to increase the switching frequency so that the other converter elements can be smaller.

The second element to be tuned is the converter inductor, presented in Figure 4.6, where typically the value of inductor can be calculated based on the specifications of the converter input voltage. However, since the input of the converter in this study is constantly changing, such calculations doesn't provide the optimal value of the inductor. The process of tuning the inductor was carried out by sweeping the inductor value in the range of 20mH to 0.3H. Table 4.3 depicts the result of this trial and error on both this study and the previous study.

In the simulations leading to these results, the internal parameter values were set by first test case and the parameters for the proposed algorithm were set to m=10, h=2, RT=5. While changing the value of inductor in each step of sweeping, the parasitic resistance of the inductance was also changing accordingly using typical inductor resistance values. To be able to compare the two studies in the same context, the duty cycle and switching frequency of the previous study (Nguyen et al., 2019) was set to a fixed value, just like the proposed method (D=70%, F_{SW}=500 Hz). The results in Table 4.3 demonstrate that the optimal inductor value for each PMS approach although can be of the same order of magnitude, are not identical.

4.2 Results and discussion

4.2.1 Without voltage regulation

Now that all the variables and parameters of the simulation are determined, we can proceed to present the results of the proposed PMS to the one of (Nguyen et al., 2019). These comparisons are carried out in two categories (with and without voltage regulation), each category comprises of two tests, one with the first test case and another one with the second test case. It

is worth noting that the only variable factor in these comparisons is the way the algorithms manage the switches in their circuits and all the other parts like circuit elements values, parasitic resistance, controller parameters, etc. are identical between the two approaches.

The first category is the power comparison of the two approaches while there is no voltage regulation, and the duty cycle is set to a constant value. Although this scenario is not practical in real applications, its importance is that apart from the usage of different PMS algorithms, nothing interferes in the mean output power. In this category, as shown in Table 4.3, while using the first test case, the highest mean output power achieved by the proposed PMS is 6.202mW using a 37.5mH inductor. The PMS from the previous study (Nguyen et al., 2019) reached its peak mean output power of 4.315mW using 50mH inductor. The results indicate an increase of 43.7% in the mean power output level transferred to the load for the proposed PMS.

Table 4.3 Mean output power at load level of the two approaches for different inductor values without voltage regulation using the first test case

L (H)	Parasitic resistance of L (Ω)	Proposed PMS			Previous study PMS (Nguyen et al., 2019)			Improvement of the P_{out} in proposed PMS
		P_{in} (mW)	P_{out} (mW)	Converter efficiency	P_{in} (mW)	P_{out} (mW)	Converter efficiency	
0.02	0.75	4.194	2.821	67%	3.522	2.353	67%	19.89%
0.034	0.75	7.159	5.899	82%	1.825	1.274	70%	363.03%
0.037	0.75	7.38	6.202	84%	1.837	1.304	71%	375.61%
0.04	0.75	7.215	6.15	85%	4.072	3.427	84%	79.46%
0.043	0.75	7.049	6.069	86%	4.325	3.709	86%	63.63%
0.05	0.75	6.626	5.773	87%	4.983	4.315	87%	33.79%
0.075	0.75	5.021	4.566	91%	4.46	4.041	91%	12.99%
0.1	1	3.919	3.64	93%	3.801	3.526	93%	3.23%
0.15	1.5	2.912	2.734	94%	2.861	2.685	94%	1.82%
0.3	3	1.83	1.693	93%	1.83	1.693	93%	0.00%

Table 4.4 Mean output power at load level of the two approaches for different inductor values without voltage regulation using the second test case

L (H)	Parasitic resistance of L (Ω)	Proposed PMS			Previous study PMS (Nguyen et al., 2019)			Improvement of the P_{out} in proposed PMS
		P_{in} (mW)	P_{out} (mW)	Converter efficiency	P_{in} (mW)	P_{out} (mW)	Converter efficiency	
0.02	0.75	4.324	2.925	68%	3.028	2.018	67%	45%
0.034	0.75	7.133	5.872	82%	3.044	2.455	81%	139%
0.037	0.75	7.331	6.148	84%	3.174	2.614	82%	135%
0.04	0.75	7.348	6.242	85%	3.581	3.002	84%	108%
0.043	0.75	7.18	6.232	87%	4.324	3.736	86%	67%
0.05	0.75	6.168	5.597	91%	3.849	3.479	90%	61%
0.075	0.75	3.803	3.508	92%	3.276	3.031	93%	16%
0.1	1	3.253	3.057	94%	2.502	2.34	94%	31%
0.15	1.5	2.061	1.908	93%	1.498	1.373	92%	39%
0.3	3	4.324	2.925	68%	3.028	2.018	67%	45%

While using the second test case, as shown in Table 4.4, the proposed algorithm reached a peak mean output power of 6.242mW using a 40mH inductor. Meanwhile, the maximum mean output power that the PMS from the prior study (Nguyen et al., 2019) achieved was 3.736mW using a 75mH inductor. As illustrated in Figure 3.4b, short disconnection of the MFC3 was simulated in the second test case, during which the former PMS (Nguyen et al., 2019) was not able to draw power from any other MFC unit as well. It is observed that the difference between the two approaches in terms of mean output power has grown from 43% using the first test case to 67% using the second test case. Although the period where only one MFC unit, out of the four total units, was disconnected constituted 4.5% of the total simulation time (63s during the total simulation time of 1400s), it led to a much bigger performance gap between the two approaches.

This difference in performance in using both test cases can be justified by the fact that during the power harvesting, the proposed PMS was able to detect MFC units which were hindering the energy harvesting and disconnected them. Given that the simulation time was 1400s, the PMS from previous study (Nguyen et al., 2019) kept all the MFC units connected at all times, whereas the proposed PMS disconnected MFCs for a total of 175s in the first test case and 374s in the second test case. Considering the fact that during this period, the discarded unit(s)

have time to recover, while using real world MFC units, the performance difference between the two algorithms can be even bigger since the effects of recovery are not presented in the simulation.

Moreover, it can be observed that the mean output power difference of the proposed PMS using the first and second test case (without voltage regulation) is only ~1%. To justify this, we need to consider that the total time that MFCs are being operated in the simulation is 1400s×4=5600s, in this case, disconnecting only one MFC for 64s would only translate to ~1% of the time MFCs are being harvested.

4.2.2 With voltage regulation

During the simulations that have been carried out until this point, the load voltage was ranging from 1.5-6.5V which is not very practical if an electronics device is planned to be connected to the output of the converter. To tackle this problem, a PID controller was implemented to regulate the voltage by manipulating the duty cycle of the converter. However, since the input voltage of the converter is dependent on volatile MFC voltage levels, the range of fluctuation in converter input is very high which makes it unpractical to attempt to have a single voltage level at the converter output. In this study, a two-level voltage regulation controlled by a PID was utilized. The control loop of the controller is presented in Figure 4.3.

The two levels of the voltage regulation are set to 2V and 3.5V based on the fact that most of low power microcontrollers can use all their functionalities when their input voltage >3.3V while their bare minimum features can function with input voltage>1.8V. The decision between these two levels is made based on the converter input voltage, considering a maximum boost ratio of 5 to keep the efficiency high. If V_{SC} is higher than 0.75V, the higher voltage regulation level is selected as a reference for the control loop, whereas if it's lower than 0.75V, the lower voltage level is selected as a reference for load voltage. Although this method would mean that the operation of the processor is dependent on the voltage, it ensures that high priority tasks are accomplished. The output of this voltage reference level is compared to the

actual load voltage and the error between reference and actual voltage is minimized by the controller in a closed loop. The value of proportional (P) and integral (I) coefficients of the controller were set by trial and error to P = 0.35 and I = 0.5. Since this controller is meant to control the duty cycle, it is important to saturate the output of the controller so it doesn't diverge from the range it is supposed to be. To keep the converter in high efficiency range, we will saturate any output higher that 0.85 and any output lower than 0.1 (based on Figure 2.8).

After setting up the voltage regulation control, the inductor sweep test is carried out again in the 20mH to 300mH range. The results are shown in Table 4.5. It is observed that the optimal inductor value with regards to converter efficiency has changed.

Table 4.5 Mean output power at load level of the two approaches
for different inductor values with voltage regulation using the first test case

L (H)	Parasitic resistance of L (Ω)	Proposed PMS			Previous study PMS (Nguyen et al., 2019)			Improvement of the P_{out} in proposed PMS
		P_{in} (mW)	P_{out} (mW)	Converter efficiency	P_{in} (mW)	P_{out} (mW)	Converter efficiency	
0.02	0.75	2.863	1.766	62%	2.809	1.738	62%	2%
0.034	0.75	2.554	1.81	71%	2.557	1.819	71%	0%
0.037	0.75	2.52	1.81	72%	2.526	1.816	72%	0%
0.04	0.75	2.488	1.809	73%	2.5	1.827	73%	-1%
0.043	0.75	2.486	1.862	75%	2.432	1.825	75%	2%
0.05	0.75	2.43	1.948	80%	2.254	1.812	80%	8%
0.075	0.75	2.491	2.059	83%	2.18	1.813	83%	14%
0.1	1	2.353	2.044	87%	2.086	1.816	87%	13%
0.15	1.5	2.123	1.897	89%	2.037	1.82	89%	4%
0.3	3	2.863	1.766	62%	2.809	1.738	62%	2%

The second category concentrates on the effect of voltage regulation in system performance. During the simulations of this category, a PID controller is managing the duty cycle to regulate voltage in two levels. The results of simulations of this category show that the highest power recorded from the proposed PMS is 2.059mW as presented in Table 4.5. This level of mean output power is achieved with inductor value of 100mH using the first test case. The PMS from the previous study reached a maximum mean output power of 1.827mW using a 40mH

inductor, which is a 13% improvement in the maximum power value of the proposed PMS compared to the former PMS.

Using the second test case while regulating voltage, demonstrates a more noticeable gap between the two approaches (Table 4.6). The proposed PMS reaches to 2.151mW at its peak using a 100mH inductor and the former PMS achieves a maximum of 1.778mW using a 50mH inductor, which is a 21% performance boost in case of the proposed PMS.

The reason behind this large change in mean output power between the first and second category simulation results is that the load that is being used is a resistive load and since its resistance is constant throughout the simulation by regulating its voltage, the output power is being limited as well. This phenomenon reduces the difference between the two PMS approaches as well.

Table 4.6 Mean output power at load level of the two approaches for different inductor values with voltage regulation using the second test case

L (H)	Parasitic resistance of L (Ω)	Proposed PMS			Previous study PMS (Nguyen et al., 2019)			Improvement of the P_{out} in proposed PMS
		P_{in} (mW)	P_{out} (mW)	Converter efficiency	P_{in} (mW)	P_{out} (mW)	Converter efficiency	
0.02	0.75	2.928	1.804	62%	2.506	1.573	63%	15%
0.034	0.75	2.641	1.873	71%	2.396	1.73	72%	8%
0.037	0.75	2.59	1.859	72%	2.376	1.733	73%	7%
0.04	0.75	2.587	1.874	72%	2.346	1.739	74%	8%
0.043	0.75	2.466	1.843	75%	2.249	1.712	76%	8%
0.05	0.75	2.692	2.146	80%	2.184	1.778	81%	21%
0.075	0.75	2.587	2.138	83%	2.036	1.705	84%	25%
0.1	1	2.48	2.151	87%	1.963	1.713	87%	26%
0.15	1.5	2.007	1.784	89%	1.989	1.772	89%	1%
0.3	3	2.928	1.804	62%	2.506	1.573	63%	15%

Figure 4.7 depicts the accuracy of the voltage regulation at load level for both approaches using first test case. It's evident that while the former PMS method is able to harvest energy, it has a steadier output voltage since there is no abrupt voltage disturbances caused by disconnection of MFC units, hence making it easier for the PI controller to regulate the output voltage. On the other hand, the supercapacitor in the proposed PMS is prone to abrupt voltage variations

since the number of connected MFCs can change at any charge-discharge cycle. Such unpredictable disturbances in boost converter input voltage are very hard to manage for the PI controller. However, if the controller and the output voltage levels are well tuned, the output voltage levels can be usable in practical applications, as presented in Figure 4.7.

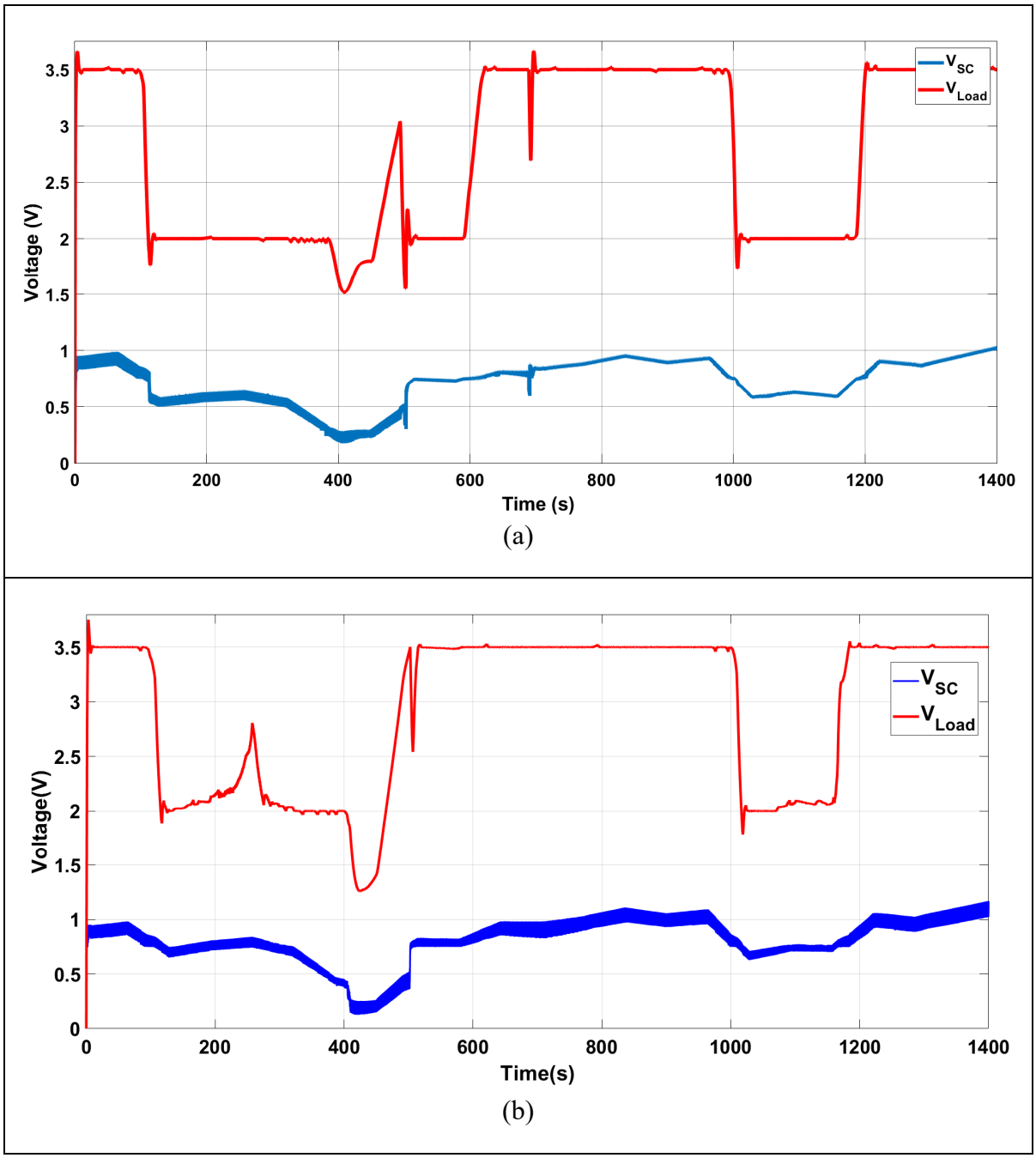

Figure 4.7 The load voltage of the two PMS approaches, while using the first test case a) proposed PMS, b) PMS from the former study (Nguyen et al., 2019)

In conclusion, chapter four provides the details of the simulation including the exact values of the various parameters used in the proposed PMS. While some of these parameters are obtained by calculation, some are selected in a reasonable range and some others are obtained from trial and error. In order to perform a fair comparison of the performance of the two PMS, simulations with identical parameters are conducted for each PMS. Simulations were first limited to the PMS including the MPPT and the converter. Then, the designed system including a voltage regulation loop was simulated. Both types of simulations were performed using the 2 test cases defined in CHAPTER 3.

CONCLUSION

The research problem that this study aims to solve is that some PMS algorithms that manage a stack of MFCS like the one previously presented in Nguyen et al. (2019), referred to as the previous PMS, can themselves be a hurdle in the way of harvesting maximum power from the stack of MFCs. Additionally, while simulating a new PMS, there is a need for a realistic test procedure (in the simulation) to be able to better evaluate and compare different PMSs before using an expensive MFC experimental setup for testing. Thus, the first objective of this paper is to design a new PMS that evaluates its decisions in regard to the potential harvestable power and chooses the solution that results in the higher power output. The second objective of this study is to develop realistic test cases that represent real-world conditions to be able to evaluate the efficacy of the proposed PMS compared to previous studies.

In the first chapter, the basics of the MFC operation are explained by discussing different types of MFCs and materials that are used in each building block of MFCs (i.e. anode, cathode, frame, etc.). The chapter proceeds to review the mathematical models available to describe the behavior of MFCs and the pros and cons of each approach. In the last section of chapter one, PMSs and voltage boosting technologies are discussed by presenting examples of some of the energy harvesting methods from previous studies.

The basic concept of the proposed PMS, limitations, and modifications made to improve the performance of the proposed PMS are discussed in the second chapter. Chapter 2 also includes the calculations related to the Discarding algorithm used to decide when we should disconnect or reconnect MFC units and the details of the voltage boosting and regulation.

Chapter three is dedicated to the experimental data acquisition and processing of that data. First, the experimental setup and details of the length and conditions of the experiment are explained. Then, the results are processed to estimate the internal parameters of the MFC electrical equivalent circuit model using the optimization method applied to the raw experimental data. Once the internal parameters of the MFC equivalent electrical circuit in various internal and ambient conditions are estimated, a scenario of the MFC behavior over a

specific period of time is constructed by concatenating the data. These scenarios also called test cases in this study, represent a series of different MFC characteristics one after another in the time domain. The idea behind constructing these test cases is to design a framework that provides equal opportunities for different PMS approaches by fixing the behavior of the MFCs during the length of the simulation. By using this framework, the PMS approaches are exposed to the same MFC behavior, making the comparison of the PMSs fair. There are two test cases created for this framework, one where all MFCs are connected and are being harvested, and the second where the MFCs have the exact same characteristics as first test case but one of the MFCs is disconnected for 4% of the total simulation time. These two test cases are called test case 1 and test case 2, respectively.

The test cases created in chapter three are fed to the simulation as inputs, and the results of the proposed PMS are compared to a previously presented PMS (Nguyen et al., 2019). The efficacy of these PMSs is investigated by comparing their mean power output during the time of simulation and the effectiveness of the voltage regulation system and the boost converter.

Chapter four discusses the simulation, results and how the proposed PMS compares to a previous PMS in terms of functionality and mean output power under various conditions. The results demonstrate that while there was no voltage regulation in the system, under test case 1, the proposed PMS peaked at 6.20mW mean output power and the previous PMS peaked at 4.32mW indicating a 44% increase in energy output. Under test case 2, the gap was even bigger where the proposed PMS still provided a maximum of 6.24mW of mean power whereas the previous PMS provided 3.74mW of mean output power to the load. The reason for this 67% performance increase is the fact that the previous PMS is not capable of delivering power in case one of the MFCs is not functioning therefore stopping the energy delivery to the load once one of the MFCs is faulty. However, the proposed PMS can simply detect the faulty MFC and discard it from the system until the MFC is functional once again, hence the difference in the mean output power of the proposed PMS between test case 1 and 2 is insignificant. Under more realistic conditions the electronic device that is being provided at the load would require voltage regulation to function properly. In the simulations with voltage regulation, under test case 1, the proposed PMS was able to deliver a maximum mean power of 2.06mW and the

previous PMS delivered a mean power of 1.83mW under optimum conditions which is a 12% performance difference. Under test case 2, the proposed PMS delivered 2.15mW of mean power whereas the previous PMS delivered 1.78mW, which is a 21% performance boost. Given these results, it is concluded that under a realistic scenario, the proposed PMS outperforms the previous PMS in terms of mean output power delivered to the load. Moreover, the voltage level at the load is stable during most of the simulations despite the large fluctuations in the MFC open circuit voltage.

While the proposed PMS is performing better than the previous PMS in terms of mean output power, there are a few drawbacks that come with this approach and need to be addressed in future studies. First, the proposed PMS uses one more switch per MFC compared to the previous PMS, which means more expensive construction, higher losses, and a higher probability of failure in the circuit. Second, the algorithm used to control the proposed PMS is computationally more demanding than the algorithm that controls the previous PMS, hence it could cause higher power consumption. Third, while discarding the MFC units that are hindering the energy harvesting process in the stack is the reason that the proposed PMS can increase the mean power output, there is no objective way to precisely know when to reconnect the discarded units. This is because when the MFC unit is connected to the system we can calculate roughly how much power is going to be delivered immediately after disconnecting the unit, but this kind of forecast is not as straightforward when the PMS is deciding whether to connect a discarded unit or not. This uncertainty can cause a chattering effect in the system when an MFC keeps getting discarded and reconnected repeatedly. In the proposed PMS, a cool-down timer and a hysteresis control method have been applied to mitigate this problem, however, this problem persists with less severity and is considered a source of potential power loss.

Given the results, it can be verified that the current study has been able to achieve the objectives discussed previously. The contributions of this study can be listed below:

- Development of a new PMS well adapted to a stack of MFCs;

- Design of a boosting and regulating voltage system which takes into consideration the specific source and the load;
- Generation of multiple test cases based on a set of experimental data extracted from 4 laboratory scale MFCs operated under various operating conditions to validate the proposed PMS.

FUTURE WORK

For future studies continuing this field of research, it can be interesting to pursue improving the proposed PMS notably to be able to have a rough idea of the energy that can potentially be provided to the system by a discarded unit before reconnecting it. This feature can minimize the potential energy loss and increase the mean output power of the system even further.

To further assess the efficacy of the proposed PMS, it needs to be tested in a real-world condition with real load and MFCs for an extended period of time. Once it is implemented in lab conditions, its costs in terms of electrical power loss due to the use extra (SWB) switches and to the higher computational effort from the microcontroller of the proposed PMS control algorithm needs to be assessed, as well.

Regarding voltage boosting and regulation, an adaptive multi-level voltage regulator could be used in order not to limit the energy harvesting process. Alternatively, for bigger loads, a battery system can be also used where the battery gets charged continuously and then the battery supplies the load in short bursts.

Finally, once the proposed PMS and voltage boosting methods have been experimentally validated, the next step can be constructing MFCs with a higher power density and harvesting them with the proposed PMS in an attempt to make an autonomous system.

BIBLIOGRAPHY

Adekunle, A., Raghavan, V., & Tartakovsky, B. (2017). Carbon source and energy harvesting optimization in solid anolyte microbial fuel cells. *Journal of power Sources, 356*, 324-330.

Behera, M., & Ghangrekar, M. á. (2009). Performance of microbial fuel cell in response to change in sludge loading rate at different anodic feed pH. *Bioresource technology, 100*(21), 5114-5121.

Chassé, F., & Woodward, L. (2016). A new approach to Particle Swarm Optimization for dynamic systems with multiple units. Paper presented at the *IECON 2016-42nd Annual Conference of the IEEE Industrial Electronics Society*.

Cheng, S., Liu, H., & Logan, B. E. (2006). Increased performance of single-chamber microbial fuel cells using an improved cathode structure. *Electrochemistry communications, 8*(3), 489-494.

Coronado, J., Perrier, M., & Tartakovsky, B. (2013). Pulse-width modulated external resistance increases the microbial fuel cell power output. *Bioresource technology, 147*, 65-70.

Coronado, J., Tartakovsky, B., & Perrier, M. (2013). On-line Monitoring and Parameter Estimation of a Microbial Fuel Cell Operated with Intermittent Connection of the External Resistor. *IFAC Proceedings Volumes, 46*(31), 233-237.

Deb, D., Patel, R., & Balas, V. E. (2020). A review of control-oriented bioelectrochemical mathematical models of microbial fuel cells. *Processes, 8*(5), 583.

Dürr, M., Cruden, A., Gair, S., & McDonald, J. (2006). Dynamic model of a lead acid battery for use in a domestic fuel cell system. *Journal of power Sources, 161*(2), 1400-1411.

Esfandyari, M., Fanaei, M. A., Gheshlaghi, R., & Mahdavi, M. A. (2016). Neural network and neuro-fuzzy modeling to investigate the power density and Columbic efficiency of microbial fuel cell. *Journal of the Taiwan Institute of Chemical Engineers, 58*, 84-91.

Esfandyari, M., Fanaei, M. A., Gheshlaghi, R., & Mahdavi, M. A. (2017). Mathematical modeling of two-chamber batch microbial fuel cell with pure culture of Shewanella. *Chemical Engineering Research and Design, 117*, 34-42.

Femia, N., Petrone, G., Spagnuolo, G., & Vitelli, M. (2005). Optimization of perturb and observe maximum power point tracking method. *IEEE Transactions on Power Electronics, 20*(4), 963-973.

Feng, Y., Wang, X., Logan, B. E., & Lee, H. (2008). Brewery wastewater treatment using air-cathode microbial fuel cells. *Applied Microbiology and Biotechnology, 78*(5), 873-880.

FuelCellsWorks. (2018, 11/11/2018). Microbial Fuel Cell Technology that turns urine into electricity commercialised through spin out company. Retrieved from https://fuelcellsworks.com/news/microbial-fuel-cell-technology-that-turns-urine-into-electricity-commercial/

Ge, Z., & He, Z. (2016). Long-term performance of a 200 liter modularized microbial fuel cell system treating municipal wastewater: treatment, energy, and cost. *Environmental Science: Water Research & Technology, 2*(2), 274-281.

Goswami, R., & Mishra, V. K. (2018). A review of design, operational conditions and applications of microbial fuel cells. *Biofuels, 9*(2), 203-220.

Halme, A., & Zhang, X. (1995). Research reports of Automation Technol. Lab. *Helsinki U. of Techno, 12*.

Hiyama, T., Kouzuma, S., & Imakubo, T. (1995). Identification of optimal operating point of PV modules using neural network for real time maximum power tracking control. *IEEE Transactions on Energy conversion, 10*(2), 360-367.

Ieropoulos, I., Greenman, J., & Melhuish, C. (2012). Urine utilisation by microbial fuel cells; energy fuel for the future. *Physical chemistry chemical physics, 14*(1), 94-98.

Ieropoulos, I., Greenman, J., Melhuish, C., & Horsfield, I. (2010). EcoBot-III-A Robot with Guts. Paper presented at the *ALIFE XII*, Odense, Denmark.

Ieropoulos, I., Melhuish, C., Greenman, J., & Horsfield, I. (2005). EcoBot-II: An artificial agent with a natural metabolism. *International Journal of Advanced Robotic Systems, 2*(4), 31.

Ieropoulos, I., Pasternak, G., & Greenman, J. (2017). Urine disinfection and in situ pathogen killing using a Microbial Fuel Cell cascade system. *PloS one, 12*(5), e0176475.

Ieropoulos, I. A., Stinchcombe, A., Gajda, I., Forbes, S., Merino-Jimenez, I., Pasternak, G., . . . Greenman, J. (2016). Pee power urinal–microbial fuel cell technology field trials in the context of sanitation. *Environmental Science: Water Research & Technology, 2*(2), 336-343.

Jiang, D., Curtis, M., Troop, E., Scheible, K., McGrath, J., Hu, B., . . . Li, B. (2011). A pilot-scale study on utilizing multi-anode/cathode microbial fuel cells (MAC MFCs) to enhance the power production in wastewater treatment. *International Journal of Hydrogen Energy, 36*(1), 876-884.

Karra, U., Muto, E., Umaz, R., Kölln, M., Santoro, C., Wang, L., & Li, B. (2014). Performance evaluation of activated carbon-based electrodes with novel power management system for long-term benthic microbial fuel cells. *International Journal of Hydrogen Energy, 39*(36), 21847-21856.

Kebir, A., Woodward, L., & Akhrif, O. (2019). Real-time optimization of renewable energy sources power using neural network-based anticipative extremum-seeking control. *Renewable Energy, 134*, 914-926.

Khaled, F., Ondel, O., & Allard, B. (2014). Optimal energy harvesting from serially connected microbial fuel cells. *IEEE Transactions on Industrial Electronics, 62*(6), 3508-3515.

Kim, J. R., Premier, G. C., Hawkes, F. R., Rodríguez, J., Dinsdale, R. M., & Guwy, A. J. (2010). Modular tubular microbial fuel cells for energy recovery during sucrose wastewater treatment at low organic loading rate. *Bioresource technology, 101*(4), 1190-1198.

Kim, Y., Jo, H., & Kim, D. (1996). A new peak power tracker for cost-effective photovoltaic power system. Paper presented at the *IECEC 96. Proceedings of the 31st Intersociety Energy Conversion Engineering Conference*.

Kottas, T. L., Boutalis, Y. S., & Karlis, A. D. (2006). New maximum power point tracker for PV arrays using fuzzy controller in close cooperation with fuzzy cognitive networks. *IEEE Transactions on Energy conversion, 21*(3), 793-803.

Kuntke, P., Śmiech, K., Bruning, H., Zeeman, G., Saakes, M., Sleutels, T., . . . Buisman, C. (2012). Ammonium recovery and energy production from urine by a microbial fuel cell. *Water research, 46*(8), 2627-2636.

Ledezma, P., Stinchcombe, A., Greenman, J., & Ieropoulos, I. J. P. c. c. p. (2013). The first self-sustainable microbial fuel cell stack. *15*(7), 2278-2281.

Lee, H.-S., Salerno, M. B., & Rittmann, B. E. (2008). Thermodynamic evaluation on H2 production in glucose fermentation. *Environmental science & technology, 42*(7), 2401-2407.

Liang, P., Huang, X., Fan, M.-Z., Cao, X.-X., & Wang, C. (2007). Composition and distribution of internal resistance in three types of microbial fuel cells. *Applied Microbiology and Biotechnology, 77*(3), 551-558.

Logan, B. E. (2008). *Microbial fuel cells*: John Wiley & Sons.

Logan, B. E. (2010). Scaling up microbial fuel cells and other bioelectrochemical systems. *Applied Microbiology and Biotechnology, 85*(6), 1665-1671.

Macdonald, J. R., & Johnson, W. B. (2018). Fundamentals of Impedance Spectroscopy. In *Impedance Spectroscopy* (pp. 1-20).

Min, B., Kim, J., Oh, S., Regan, J. M., & Logan, B. E. (2005). Electricity generation from swine wastewater using microbial fuel cells. *Water research, 39*(20), 4961-4968.

Mitov, M., Bardarov, I., Mandjukov, P., & Hubenova, Y. (2015). Chemometrical assessment of the electrical parameters obtained by long-term operating freshwater sediment microbial fuel cells. *Bioelectrochemistry, 106*, 105-114.

Mukherjee, A., Patel, V., Shah, M. T., Jadhav, D. A., Munshi, N. S., Chendake, A. D., & Pant, D. J. J. o. P. S. (2022). Effective power management system in stacked microbial fuel cells for onsite applications. *517*, 230684.

Mumtaz, F., Yahaya, N. Z., Meraj, S. T., Singh, B., Kannan, R., & Ibrahim, O. (2021). Review on non-isolated DC-DC converters and their control techniques for renewable energy applications. *Ain Shams Engineering Journal, 12*(4), 3747-3763.

Nguyen, C.-L., Tartakovsky, B., & Woodward, L. (2019). Harvesting energy from multiple microbial fuel cells with a high-conversion efficiency power management system. *ACS Omega, 4*(21), 18978-18986.

Oliveira, V., Simões, M., Melo, L., & Pinto, A. (2013). A 1D mathematical model for a microbial fuel cell. *Energy, 61*, 463-471.

Osiris, B. F. (2017). *CONVERSION OPTIMALE DE LA PUISSANCE FOURNIE PAR UNE PILE À COMBUSTIBLE MICROBIENNE*. Montreal, QC. École de technologie supérieure.

Pandey, A., Dasgupta, N., & Mukerjee, A. K. (2008). High-performance algorithms for drift avoidance and fast tracking in solar MPPT system. *IEEE Transactions on Energy conversion, 23*(2), 681-689.

Park, D. H., & Zeikus, J. G. (2003). Improved fuel cell and electrode designs for producing electricity from microbial degradation. *Biotechnology and Bioengineering, 81*(3), 348-355. doi:https://doi.org/10.1002/bit.10501

Picioreanu, C., Head, I. M., Katuri, K. P., van Loosdrecht, M. C., & Scott, K. (2007). A computational model for biofilm-based microbial fuel cells. *Water research, 41*(13), 2921-2940.

Picioreanu, C., Katuri, K. P., van Loosdrecht, M., Head, I. M., & Scott, K. (2010). Modelling microbial fuel cells with suspended cells and added electron transfer mediator. *Journal of applied electrochemistry, 40*(1), 151-162.

Pinto, R., Srinivasan, B., Manuel, M.-F., & Tartakovsky, B. (2010). A two-population bio-electrochemical model of a microbial fuel cell. *Bioresource technology, 101*(14), 5256-5265.

Potter, M. C. (1911). Electrical effects accompanying the decomposition of organic compounds. *Proceedings of the royal society of London. Series b, containing papers of a biological character, 84*(571), 260-276.

Rabaey, K., Van de Sompel, K., Maignien, L., Boon, N., Aelterman, P., Clauwaert, P., . . . Verhaege, M. (2006). Microbial fuel cells for sulfide removal. *Environmental science & technology, 40*(17), 5218-5224.

Recio-Garrido, D., Perrier, M., & Tartakovsky, B. (2016). Combined bioelectrochemical–electrical model of a microbial fuel cell. *Bioprocess and biosystems engineering, 39*(2), 267-276.

Santoro, C., Arbizzani, C., Erable, B., & Ieropoulos, I. (2017). Microbial fuel cells: From fundamentals to applications. A review. *Journal of power Sources, 356*, 225-244.

Shantaram, A., Beyenal, H., Veluchamy, R. R. A., & Lewandowski, Z. (2005). Wireless sensors powered by microbial fuel cells. *Environmental science & technology, 39*(13), 5037-5042.

Silveston, P., Hudgins, R. R., & Renken, A. (1995). Periodic operation of catalytic reactors—introduction and overview. *Catalysis Today, 25*(2), 91-112.

Solodovnik, E. V., Liu, S., & Dougal, R. A. (2004). Power controller design for maximum power tracking in solar installations. *IEEE Transactions on Power Electronics, 19*(5), 1295-1304.

UWE-Bristol. (2018, 23/4/2018). PEE POWER® to light up more sites after Africa school trial success. Retrieved from https://info.uwe.ac.uk/news/uwenews/news.aspx?id=3790

Wang, H., Park, J.-D., & Ren, Z. J. (2015). Practical Energy Harvesting for Microbial Fuel Cells: A Review. *Environmental science & technology, 49*(6), 3267-3277. doi:10.1021/es5047765

Wang, J., Zheng, T., Wang, Q., Xu, B., & Wang, L. (2015). A bibliometric review of research trends on bioelectrochemical systems. *Current Science*, 2204-2211.

Woodward, L., Tartakovsky, B., Perrier, M., & Srinivasan, B. (2009). Maximizing power production in a stack of microbial fuel cells using multiunit optimization method. *Biotechnology progress, 25*(3), 676-682.

Yang, F., Zhang, D., Shimotori, T., Wang, K.-C., & Huang, Y. (2012). Study of transformer-based power management system and its performance optimization for microbial fuel cells. *Journal of power Sources, 205*, 86-92.

Yu, G., Jung, Y., Choi, J., & Kim, G. (2004). A novel two-mode MPPT control algorithm based on comparative study of existing algorithms. *Solar Energy, 76*(4), 455-463.

Zhang, D., Yang, F., Shimotori, T., Wang, K.-C., & Huang, Y. (2012). Performance evaluation of power management systems in microbial fuel cell-based energy harvesting applications for driving small electronic devices. *Journal of power Sources, 217*, 65-71.

Zhang, X.-C., & Halme, A. (1995). Modelling of a microbial fuel cell process. *Biotechnology Letters, 17*(8), 809-814.

Zhang, X., Ren, H., Pyo, S., Lee, J.-I., Kim, J., & Chae, J. (2014). A high-efficiency DC–DC boost converter for a miniaturized microbial fuel cell. *IEEE Transactions on Power Electronics, 30*(4), 2041-2049.

Zhuang, L., Zheng, Y., Zhou, S., Yuan, Y., Yuan, H., & Chen, Y. (2012). Scalable microbial fuel cell (MFC) stack for continuous real wastewater treatment. *Bioresource technology, 106*, 82-88.

Zouggari Ben El Khyat, C. (2022). *Engineering liposomes using microfluidic devices to model cancer-derived extracellular vesicles (EV).* École de technologie supérieure, Montreal, Canada.